Regulation of signal transduction pathways by hypoxia in breast cancer subtypes

Liu, Q.

Chapter 5

Hypoxia triggers TAZ phosphorylation in basal A triple negative breast cancer cells

Qiuyu Liu, Wanda van der Stel, Vera E. van der Noord, Hanneke Leegwater, Bircan Coban, Kim Elbertse, Joannes T.M. Pruijs, Olivier J.M. Béquignon, Gerard van Westen, Sylvia E. Le Dévédec[#], Erik H.J. Danen[#]

[#]Co-corresponding authors
International Journal of Molecular Sciences
https://doi.org/10.3390/ijms231710119

Abstract
Hypoxia and HIF signaling drive cancer progression and therapy resistance and have been demonstrated in breast cancer. To what extent breast cancer subtypes differ in their response to hypoxia has not been resolved. Here, we show that hypoxia similarly triggers HIF1 stabilization in luminal and basal A triple negative breast cancer cells and we use high throughput targeted RNA sequencing to analyze its effects on gene expression in these subtypes. We focus on regulation of YAP/TAZ/TEAD targets and find overlapping as well as distinct target genes being modulated in luminal and basal A cells under hypoxia. We reveal a HIF1 mediated, basal A specific response to hypoxia by which TAZ, but not YAP, is phosphorylated at Ser89. While total YAP/TAZ localization is not affected by hypoxia, hypoxia drives a shift of [p-TAZ(Ser89)/ p-YAP(Ser127)] from the nucleus to the cytoplasm in basal A but not luminal breast cancer cells. Cell fractionation and YAP knock-out experiments confirm cytoplasmic sequestration of p-TAZ(Ser89) in hypoxic basal A cells. Pharmacological and genetic interference experiments identify c-Src and CDK3 as kinases involved in such phosphorylation of TAZ at Ser89 in hypoxic basal A cells. Hypoxia attenuates growth of basal A cells and the effect of Verteporfin, a disruptor of YAP/TAZ-TEAD–mediated transcription, is diminished under those conditions, while expression of a TAZ-S89A mutant does not confer basal A cells with a growth advantage under hypoxic conditions, indicating that other hypoxia regulated pathways suppressing cell growth are dominant.

Keywords: hypoxia, breast cancer, TAZ, phosphorylation, basal A triple negative cells

Introduction

Breast cancer represents a heterogeneous disease with several intrinsic molecular subtypes. A major distinction can be made by referring to the cell type of origin, with HER2-enriched, luminal A, and luminal B breast cancers arising from the luminal epithelial compartment and basal-like breast cancers arising from the basal/myoepithelial cell compartment [1]. Luminal A has a relatively good prognosis and luminal B breast cancer has higher Ki-67 expression and chromosomal instability and is associated with a less favorable prognosis [2–5]. Basal-like breast cancers can be subdivided in basal A and B, based on epithelial (basal A) or more mesenchymal characteristics (basal B) including differences in expression of cell adhesion receptors such as E-cadherin and claudins and most basal-like breast cancers are triple negative breast cancer (TNBC): they lack estrogen receptor and progesterone receptor and do not overexpress HER2. Triple negative breast cancer is the most aggressive subtype with frequent metastasis and for which targeted therapies are lacking [6–9].

In addition to genetic and epigenetic alterations driving initiation and progression of cancer, cross talk between tumor cells and their tissue microenvironment controls primary tumor growth, tissue invasion, and metastatic colonization [10,11]. One aspect of the microenvironment surrounding cancer cells in solid tumors is its hypoxic nature [12,13]. While hypoxia initially poses a restriction to tumor growth, tumors ultimately escape from this barrier and there is clinical evidence pointing to hypoxia as a driver of tumor progression and therapy resistance [14–16]. Tumor cells as well as various cell types in the tumor microenvironment adapt gene expression patterns in response to hypoxia, predominantly through the hypoxia-inducible factor (HIF) family of transcription factors. Central in this response is the stabilization of a transcription complex consisting of HIF1α or HIF2α and aryl hydrocarbon nuclear translocator (ARNT; a.k.a. HIF1B). HIF1/2α is ubiquitinated and targeted for degradation by the Von Hippel-Lindau (VHL) E3 ubiquitin ligase complex under normoxia. Under hypoxia, degradation domains in HIF1/2α are not hydroxylated by oxygen-dependent prolyl hydroxylases, thus preventing recognition by VHL and causing stabilization of HIF1/2α and its concentration in the nucleus, formation of the HIF/ARNT complex, and transcriptional activation of HIF target genes [17,18]. In addition, hypoxia-independent mechanisms have been identified that can trigger HIF signaling in normal and cancer cells [12].

Tumor hypoxia has been extensively demonstrated in breast cancer [19] and expression of HIF1α represents an independent factor for poor prognosis in patients with lymph node-negative and -positive breast cancer, including several different subtypes [20–24]. Hypoxia impacts on a variety of other signaling pathways downstream of- or in parallel to HIF signaling. It has been shown that hypoxia can affect expression, localization or activity of Yes-associated protein 1 (YAP) and WW-domain-containing transcription regulator 1 (WWTR1; a.k.a. TAZ). YAP and TAZ are transcriptional co-activators that regulate gene transcription in complex with members of the TEA domain (TEAD) family [25]. YAP/TAZ activity is regulated at the level of gene expression, protein degradation, and nuclear/cytoplasmic distribution. One critical event is phosphorylation of YAP and TAZ, which shifts the balance towards cytoplasmic localization where interactions with 14-3-3 proteins target them to proteasomal degradation. Multiple inputs, including activity of LATS1/2 kinases in the Hippo signaling cascade, cell adhesion and polarity, extracellular

forces, cell metabolism and growth factors control YAP/TAZ phosphorylation, nuclear localization, and interaction with TEADs to activate transcription [25,26]. Reduced YAP/TAZ nuclear localization in response to long term inhibition of prolyl hydroxylase domain enzymes in renal tubular cells was proposed to involve HIF signaling [27]. Increased phosphorylation of TAZ under hypoxia was reported to occur independent of LATS1 in ovarian cancer cells [28]. In breast cancer cells, HIF1 was reported to regulate expression and localization of TAZ and an interaction between - and reciprocal activation of - HIF1 and TAZ was shown [29,30].

It is currently not known to what extent signaling responses to hypoxia differ between different breast cancer subtypes. Here, we investigate the response to hypoxia in a series of luminal and basal A breast cancer cell lines. We find that HIF1α stabilization is similarly activated and triggers overlapping as well as distinct changes in gene expression including YAP/TAZ/TEAD target genes in these subtypes. Strikingly, HIF1 mediated phosphorylation of TAZ, but not YAP, at a site known to promote its cytoplasmic sequestration and proteasomal degradation, is observed in all basal A cell lines tested but not in any of the luminal breast cancer cell lines. Such basal A specific phosphorylation does not involve activation of the Hippo signaling cascade. Instead, we identify Src and CDK3 as kinases involved in phosphorylation of TAZ in basal A cells under hypoxia and we explore the impact on TAZ localization.

Experimental procedures

Cell culture, reagents, and antibodies

Human breast cancer cell lines representing luminal-like (MCF7, T47D, BT474) and basal A (HCC1806, HCC1143 and SUM149PT) subtypes were obtained from the American Type Culture Collection. Cells were cultured in RPMI1640 medium with 10% fetal bovine serum, 25 U/mL penicillin and 25 µg/mL streptomycin in the incubator (37°C, 5% CO_2). For normoxia 21% O_2 was used and for hypoxia 1% O_2 was used. For experiments, initial seeding cell densities for different cell lines were adjusted to ensure the final cell confluency was similar at the experimental endpoint. Medium was not refreshed in order not to disturb the hypoxic environment. O_2 concentration in the incubator was frequently monitored. HIF1α nuclear stabilization and CA9 induction were measured to verify hypoxia.

Primary antibodies (Abs) included those targeting Carbonic Anhydrase IX (NB100-417SS; Novus, Englewood, CO, USA), p-YAP/p-TAZ (#13008; Cell Signaling Technology, Danvers, MA, USA), YAP (#4912; Cell Signaling Technology), TAZ (#83669; Cell Signaling Technology), Src (#2108; Cell Signaling Technology), p-Src (#6943; Cell Sig-naling Technology), HIF1α (#610959; BD Biosciences, Franklin Lakes, NJ, USA), GAPDH (sc-32233; Santa Cruz, Dallas, TX, USA), β-actin (sc-47778; Santa Cruz), Tubulin (T-9026; Sigma-Aldrich, Burlington, MA, USA). For immune fluorescence microscopy, secondary Abs were Alexa 488–linked anti-mouse IgG (Invitrogen, Waltham, MA, USA) and Alexa 546–linked anti-rabbit IgG (Invitrogen). For Western blotting, secondary Abs included horseradish peroxidase (HRP)–linked anti-rabbit or mouse IgG (Jackson ImmunoResearch Laboratories Inc., West Grove, PA, USA).

Hoechst was purchased from Thermo Fisher, Waltham, MA, USA. BV02, Verteporfin and

DMOG were purchased from Sigma-Aldrich. PP2 and Dasatinib were purchased from Selleckchem, Planegg, Germany.

Sulforhodamine B (SRB) assay
SRB assays were used to measure cell proliferation. 3000-5000 cells/well were seeded in 96-well plates. At indicated time points, 50% TCA was used to fix the plates and 0.4% SRB was added and incubated at RT avoiding light. Plates were washed with 1% acetic to remove unbound SRB and air dried. 10mM Tris was added into wells to extract protein and absorbance was measured at 540nm by plate reader (Tecan Infinite M1000, Männedorf, Switzerland).

Gene silencing, deletion, and ectopic expression
For transient siRNA mediated gene silencing 50nM SMARTpool siGENOME siRNAs (siRNAs (Dharmacon, Lafayette, CO, USA) were transfected using the transfection reagent INTERFERin (Polyplus, Illkirch-Strasbourg, France) according to the manufacturer's procedures. Controls included a SMARTpool targeting the luciferase gene, GAPDH, and a mixture of siRNAs from the whole genome library targeting all kinases in the human genome, diluted to the same total siRNA concentration as used for the SMARTpools (kinase pool).

Lentiviral supernatants were generated in HEK293 cells and used for transduction of target cells in combination with 5 μg/ml polybrene. For stable gene silencing, cells were transduced using lentiviral shRNA vectors (LentiExpress; Sigma-Aldrich, Saint Louis, MO, USA). Transduced cells were selected in medium containing puromycin. An shRNA targeting enhanced green fluorescent protein (eGFP) served as control.

For CRIPSR/Cas9 knockout, cells were transduced with lentiviral Edit-R Tre3G promotor-driven Cas9 (Dharmacon) and selected by blasticidin. Limited dilution was used to generate Cas9 monoclonal cells. Subsequently, Cas9-monoclonal cells were transduced with U6-gRNA: hPGK-puro-2A-tBFP containing control non-targeting or YAP targeting sgRNAs (Sigma) and bulk selected by puromycin. Knockout was induced by exposure to doxycycline for 48 hours.

For ectopic expression of TAZ-S89A, a lenti-TAZ-S89A-IRES-GFP lentiviral construct was kindly provided by Gangyin Zhao and Ewa Snaar Jagalska, Leiden University, and verified by sequence analysis. Cells were transduced and bulk sorted by fluorescence-activated cell sorting (FACS; Sony, SH800S Cell Sorter, San Jose, CA, USA). Sorted cells were cultured for 2 days prior to use in experiments.

Western blot, cell fractionation and immunofluorescence microscopy
For Western blot, cells were lysed with RIPA buffer containing 1% protease/phosphatase inhibitor cocktail (PIC, Sigma-Aldrich, P8340). Samples were separated by SDS–polyacrylamide gel electrophoresis and transferred to PVDF membranes (Millipore), incubated with primary Abs overnight at 4 °C followed by HRP-labelled secondary Abs (Jackson ImmunoResearch Laboratories Inc., West Grove, PA, USA) for 1 hour at RT, and imaged with enhanced chemiluminescence substrate mixture (ECL Plus, Amersham, GE Healthcare, Chicago, IL, USA). Blots were imaged using an Amersham Imager (GE

Healthcare Life Science, Chicago, IL, USA).

For cell fractionation, cells were lysed using the FractionPREP Cell Fractionation Kit (BioVision, Waltham, MA, USA) according to the manufacturer's procedures.

For immunofluorescence microscopy, cells were fixed in 4% paraformaldehyde, permeabilized in 0.3% Triton X-100, blocked with 0.5% BSA for 30 min, and incubated with primary Abs overnight at 4 °C. The next day, cells were incubated with fluorescently labelled secondary Abs in combination with Hoechst33258 nuclear staining for 1 h under RT avoiding light. Images were taken with Nikon Eclipse Ti microscope and analyzed using the Intensity Ratio Nuclei Cytoplasm Tool (RRID:SCR_018573) in ImageJ (https://imagej.nih.gov/ij/). For quantitative image analysis ≥4 field of views were used per biological replicate. Scale bars shown in images represent 50 µm.

TempO-Seq and RT-qPCR

For TempO-Seq, 3000-5000 cells/well were plated in 96-well plates and incubated 5 days under normoxia or hypoxia after which the wells were washed once with cold PBS and lysed using TempO-Seq lysis buffer (Bioclavis) for 15 min at RT. Samples were stored at -80 ˚C before shipping to BioClavis for whole genome TempO-Seq analysis [63]. Expression data were shown as counts per probe. An in-house R script was used for count normalization and determining differential gene expression. The library size (total number of reads per sample) was set as 100.000 reads and samples below this size were removed. DESeq2 package was used to normalize counts and calculate differentially expressed genes (DEGs). DEGs were filtered by $|\log_2 \text{Foldchange}| > 1$ and adjusted p-value (padj) < 0.05.

For RT-qPCR, total RNA was isolated by RNeasy Plus Mini Kit (Qiagen) and cDNA was synthesized by the RevertAid H Minus First Strand cDNA Synthesis Kit (Thermo Fisher Scientific, Waltham, MA, USA). Real-time qPCR was performed in triplicate using SYBR Green PCR (Applied Biosystems, Waltham, MA, USA) on QuantStudioTM 6 Flex Real-Time PCR system (Applied Biosystems). The following qPCR primer sets were used: β-actin forward (fw), 5'-ATTGCCGACAGGATGCAGAA-3'; β-actin reverse (rev), 5'-GCTGATCCACATCTGCTGGAA-3';CDK3forward(fw),5'-TTCCTGGTCCACTTAGGGAAG-3'; CDK3 reverse (rev), 5'-CCAGCTCTTTCGTATCTTTCGT-3'. CTGF forward (fw), 5'-GTTTGGCCCAGACCCAACTA-3'; CTGF reverse (rev), 5'- GGCTCTGCTTCTCTAGCCTG-3'; AXL forward (fw), 5'-CGTAACCTCCACCTGGTCTC-3'; AXL reverse (rev), 5'-TCCCATCGTCTGACAGCA-3'; CYR61 forward (fw), 5'-AAGAAACCCGGATTTGTGAG-3'; CYR61 reverse (rev), 5'-GCTGCATTTCTTGCCCTTT-3'. Relative mRNA expression was calculated after correction for the control (β-actin) using the $2^{-\Delta\Delta CT}$ method.

RNA-Seq and TempO-Seq data analysis in cell lines and clinical samples

Known YAP/TAZ target genes were identified from existing literature [36,37]. TEAD1-4 binding genes were identified by transcription factor enrichment analysis using the DoRothEA tool version 2 (https://dorothea.opentargets.io/#/, accessed on 14 April, 2021) [64] with log2 normalized values as input as we have described previously [65]. In short, an average fold change was calculated over all probes for each gene and used to determine z-scores (hypoxia versus normoxia). The Viper package was used to

determine transcription factor enrichment providing a normalized enrichment score per transcription factor [66]. For complete hierarchical clustering genes were uploaded to the OmicStudio tools at https://www.omicstudio.cn/tool (accessed on 13 June, 2021). RNA-seq data for a panel of 52 breast cancer lines [33] was used to identify DEGs in distinct breast cancer subtypes (basal A, basal B and luminal). RNA sequencing data from The Cancer Genome Atlas (TCGA) was obtained using the January 2017 version of TCGA Assembler R package [67]. The log2 normalized values were used for further analyzing. Data from solid primary tumor tissue samples were used [68]. Gene expression in different subtypes (ERpos and TNBC) was plotted in R v.3.6.3.

Breast Invasive Carcinoma mRNA expression from the same TCGA breast cancer study with metadata from basal-like, luminal A and luminal B breast cancer subtypes [69] was downloaded from cBioPortal [70]. Correlations of HIF1A with YAP1 and HIF1A with WWTR1 (NCBI Gene IDs: 3091, 10413 and 25937) were plotted using tidyverse, cowplot and patchwork in R v.4.1.2.

Gene set enrichment analysis (GSEA) was performed using OmicStudio tools at https://www.omicstudio.cn/tool (accessed on 12 July, 2020). Further enrichment analysis was performed using the Metascape platform (https://metascape.org, accessed on 10 May, 2020) [71].

Kinase-substrate predictions of PP2 and Dasatinib

Activity values of human kinase proteins were collected from ChEMBL (version 27) [72] by filtering with taxon identifier and protein classification level 2 set to 9606 and "Kinases" respectively. Records with unassigned pChEMBL values and molecules with molecular weight greater than 800 Da were discarded. The dataset consisted in 311,249 compound-protein interactions from 124,307 compounds and 422 kinases. Molecules were represented with 67 Pipeline Pilot molecular descriptors (Table S1) and kinase sequences with autocross-covariances [73] and domain averages [74] of BLOSUM [75], ProtFP [76], SSIA AM1 [77] and Z-scales [78] protein descriptors. Autocross-covariances were computed with a lag of 20 amino acids. For domain averages, protein sequences were split into 50 equal parts - where part length differed based on protein length. For each part the mean average value of each dimension was calculated, and the global mean average added, yielding + 1 values, where is the dimension of each protein descriptor (e.g., for the BLOSUM descriptor). A training and holdout test set were derived using 70 and 30% of the data respectively. An Extreme Gradient Boosting [79] (XGBoost version 1.4.2) regressor was fitted using 5-fold cross-validation with the following parameters: 100 maximum trees, learning rate of 0.3, max depth of 7, descriptor fraction of 0.7 and data fraction of 1.0. This proteochemometric model had an average cross-validated coefficient of determination (R^2) of 0.66, Spearman rank correlation coefficient of 0.81 and root-mean-square error (RMSE) of 0.84. When evaluated on the holdout test set, the model had Pearson correlation of 0.68, Spearman r of 0.65 and RMSE of 0.99. Affinities were then derived for the 422 kinases for the structure of PP2 and Dasatinib using the model and sorted decreasingly (Table S1).

Statistics

Data were analyzed with Student's t-test or One-way ANOVA using GraphPad Prism 7

with the exception of statistical analysis of clinical samples where Wilcoxon signed-rank test was used as indicated in figure legends.

Results

Shared and distinct responses to hypoxia in luminal and basal A breast cancer cells

To determine how luminal breast cancer and basal A cells respond to hypoxia, 3 luminal and 3 basal-A type breast cancer cell lines were cultured for 1, 3 and 5 days respectively under normoxic (21% O_2) or hypoxic (1% O_2) conditions. Hypoxia suppressed growth of MCF7 and had no effect on growth of the other two luminal cell lines (Fig 1A). By contrast, growth of all tested basal A cells was markedly attenuated under hypoxia. To explore activation of HIF signaling in these cells, HIF1α stabilization and transcriptional activation of HIF target genes was analyzed. HIF1α stabilization and nuclear localization were similarly induced after 1 and 3 days under hypoxia throughout the panel of luminal and basal A cell lines (Fig 1B, Fig S1). Likewise, protein expression of the hypoxic biomarker CA9, a HIF1 regulated gene encoding a carbonic anhydrase isoenzyme was induced at 3- and 5-day hypoxia in all cell lines tested (Fig 1C). Next, TempO-Seq, a high-throughput targeted sequencing technology was used to determine genome wide changes in RNA expression in a luminal and basal A cell line in response to 5 days growth in hypoxia. Using a cutoff of [$|Log_2 Foldchange| > 1$; padj < 0.05], ~2000 versus ~5000 hypoxia responsive genes were identified in MCF7 and HCC1143, respectively (Table S2). This set contained a series of previously published HIF1 responsive genes [31] that partly overlapped between the two cell lines, including a shared strong upregulation of CA9 (Fig 1D). GSEA and Metascape identified shared hypoxia induced changes including those in pathways regulating cell cycle progression and extracellular matrix turnover in luminal and basal A cells (Fig S2, S3). Notably, while the response to hypoxia was the most enriched term identified by Metascape in MCF7 (Fig S2) it was not among the 20 most enriched terms in HCC1143 (Fig S3). Rather, in HCC1143 terms associated with adhesion and migration were prominent. Together, this data shows that hypoxia triggers HIF1 stabilization in luminal and basal A cells and causes overlapping as well as distinct changes in gene expression.

Expression of YAP/TAZ/TEAD complex in breast cancer subtypes and response to hypoxia

Cross talk between hypoxia and YAP/TAZ signaling has been reported [32]. Analyzing RNA-Seq data for a panel of 52 human breast cancer cell lines [33], we observed a significant increase in YAP and especially WWTR1 (encoding TAZ) expression in basal A cell lines as compared to luminal cell lines (Fig 2A). Accordingly, by exploring RNA-Seq data from breast cancer patients [34,35], we show that expression of YAP and especially WWTR1 was increased in TNBC tumors as compared to ER positive tumors (Fig 2B). The TEAD transcription factors that associate with YAP/TAZ transcriptional coactivators in the Hippo pathway did not differ between TNBC and luminal cell lines but TEAD3 was significantly lower in basal-B TNBC cell lines as compared to basal-A and luminal cell lines (Fig S4A). However, this association was not corroborated in clinical samples where, in fact, TEAD2-4 were all increased in TNBC tumors as compared to ER positive tumors (Fig S4B). A positive correlation of expression of YAP and WWTR1 with expression of HIF1A was detected in breast cancer patients, with particularly high expression of all three genes in basal-like tumors (Fig 2C). The analysis of our TempO-Seq data did

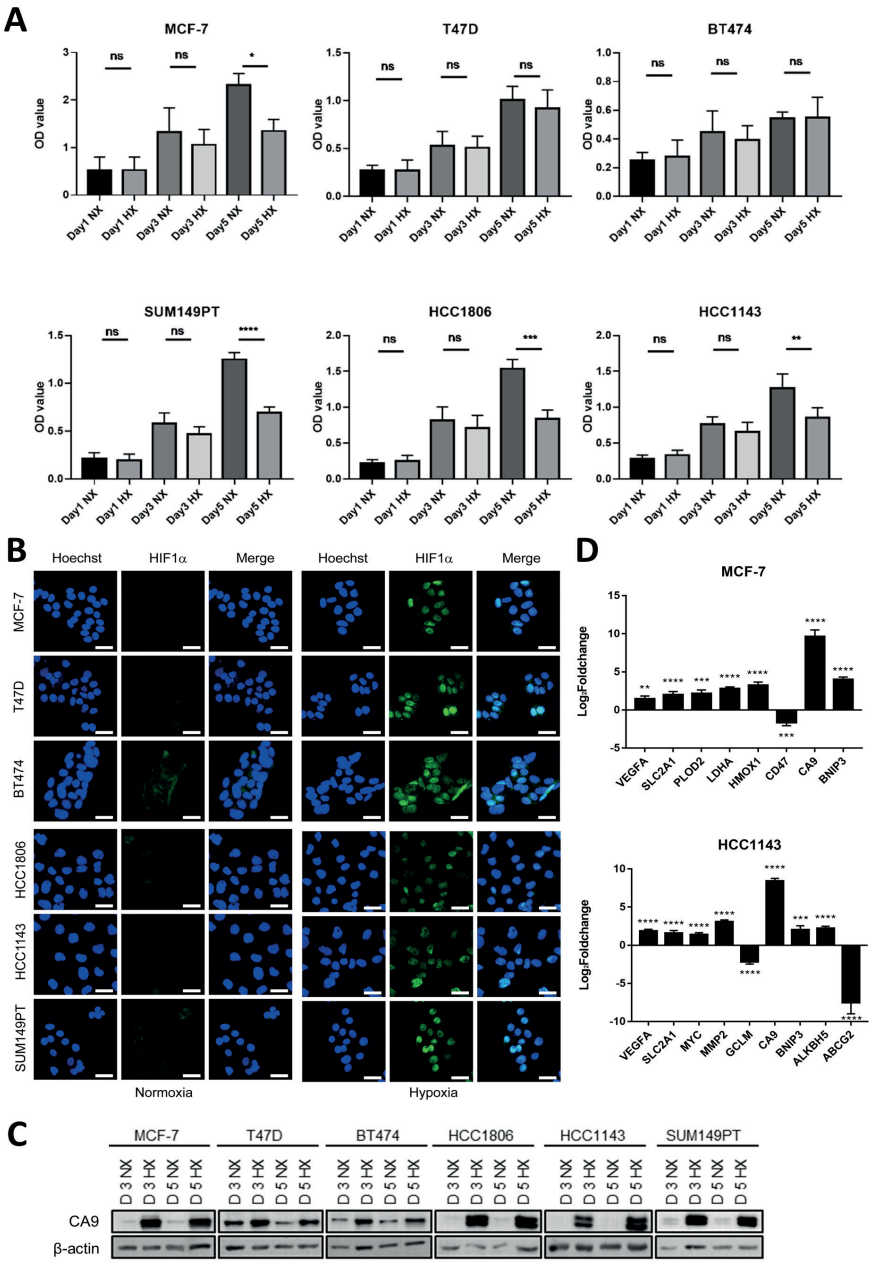

Figure 1. Modulation of cell growth and activation of HIF signaling in response to hypoxia in a series of luminal and basal A cell lines. (A) Cell growth analyzed by SRB for three luminal (MCF7, T47D and BT474) and three basal A (SUM149PT, HCC1806 and HCC1143) breast cancer cell lines grown under normoxia (21% O_2; NX) or hypoxia (1% O_2; HX) for 1, 3 or 5 days. Mean and SD of OD values from three biological replicates performed in triplicate are shown. ns, non-significant; *, p<0.05; **, p<0.01; ***, p<0.001; ****, p<0.0001; ns, not significant. **(B)** Luminal and basal A cell lines incubated under normoxia or hypoxia for 3 days analyzed for HIF1α expression and localization by confocal immunofluorescence microscopy. Blue, Hoechst; Green, HIF1α Ab. One representative experiment of three biological replicates is shown. **(C)** CA9 expression analyzed by Western blot after 3 and 5-day incubation under normoxia or hypoxia for

the indicated luminal and basal A cell lines. **(D)** Identification of known HIF1 responsive genes [51] in TempO-Seq data comparing 5-day incubation under normoxia or hypoxia in MCF7 and HCC1143 cells. Mean Log_2Foldchange for hypoxia relative to normoxia and SD of triplicate measurements is shown. **, padj<0.01; ***, padj<0.001; ****, padj<0.0001.

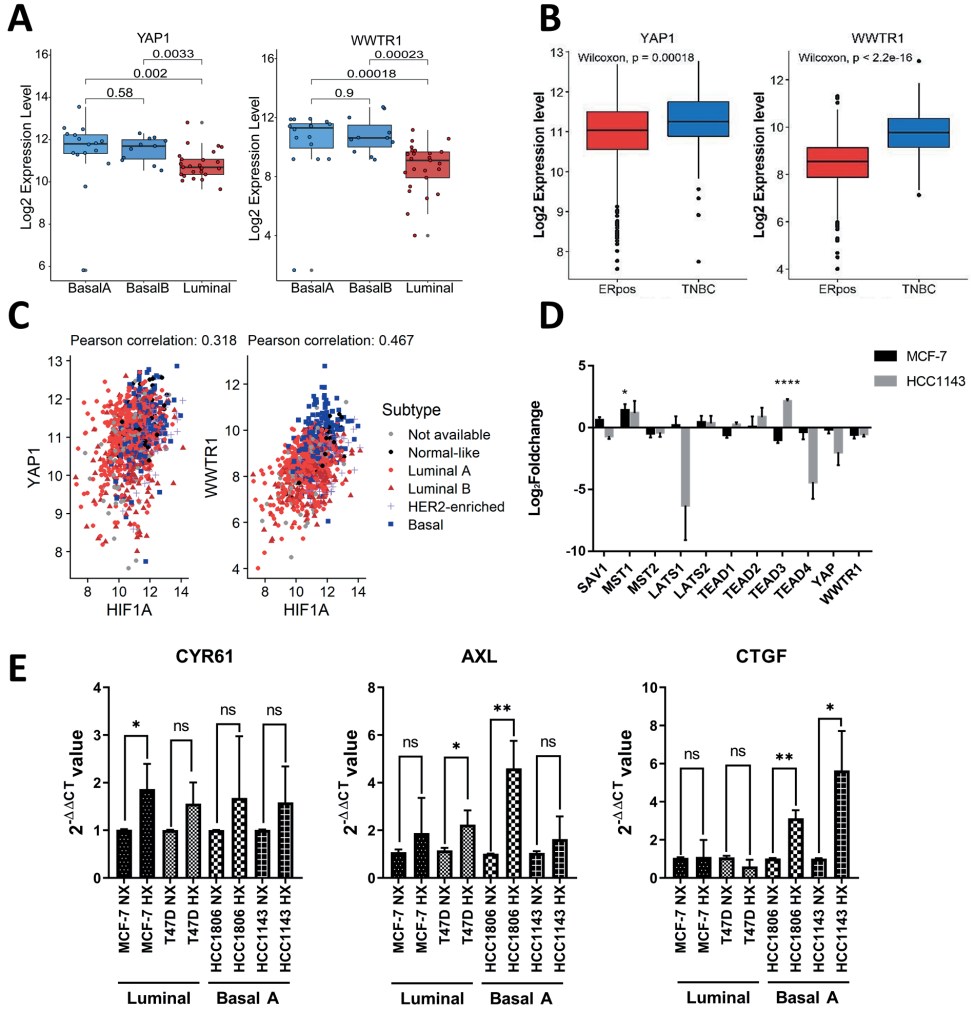

Figure 2. Expression of YAP and TAZ in breast cancer cell lines and tumors. (A) RNA expression level of YAP and TAZ (WWTR1) from RNA-Seq data for 52 human breast cancer cell lines classified by luminal-, basal A-, or basal B-like subtype [37]. p-value calculated using One-way ANOVA. **(B)** Log_2RNA expression levels of YAP and TAZ in ER positive and TNBC clinical samples. p-value calculated using Wilcoxon signed-rank test. **(C)** Correlation between RNA expression levels for HIF1α and YAP and for HIFα and TAZ determined using cBioPortal data from basal-like, HER2 enriched, luminal A and luminal B breast cancer subtypes. **(D)** Expression of YAP, TAZ, TEAD1-4, and upstream kinases in the Hippo signaling cascade determined in TempO-Seq data. Log_2Foldchange under hypoxia relative to normoxia is shown in MCF7 and HCC1143. Mean and SD of triplicate measurements is shown. *, padj<0.05; ****, padj<0.0001. **(E)** qPCR experiment showing expression of the indicated YAP/TAZ targets genes in the indicated luminal and basal A TNBC cell lines exposed to normoxia or hypoxia after 5 days. Mean expression relative to β-actin is shown. Error bars indicate SD for triplicate measurements. *, p<0.05; **, p<0.01; ns, not significant.

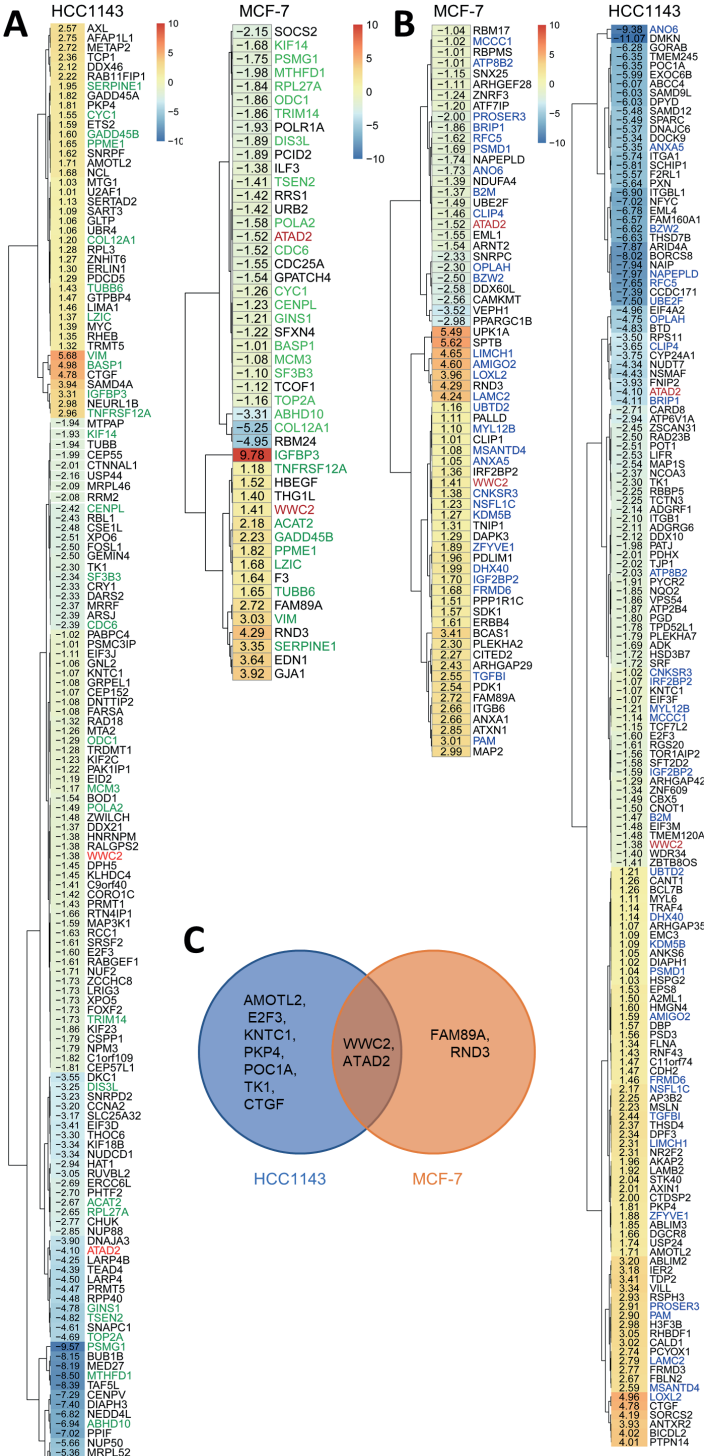

Figure 3. Identification of candidate YAP/TAZ/TEAD target genes in hypoxia-responsive genes in MCF7 and HCC1143 cells. (A, B) Heatmaps showing intersection of TempO-Seq data for hypoxia-regulated genes in MCF7 and HCC1143 cells with YAP/TAZ/TEAD target genes reported in literature (A; [32,33]) and candidate TEAD1-4-binding genes identified using DoRothEA (B; [55]). Values are Log_2 Foldchange under hypoxia relative to normoxia. Genes labeled green in (A) or labeled blue in (B) are shared between MCF7 and HCC1143 in the respective analyses. Genes labeled red in (A) and (B) are shared in both analyses for both cell lines. **(C)** Venn diagram showing distinct and overlapping hypoxia regulated genes for MCF7 and HCC1143 identified both in literature and by DoRothEA.

not detect significant hypoxia-induced changes in RNA expression of YAP/TAZ/TEAD complex members except for an increase in TEAD3 in HCC1143 cells (Fig 2D). Moreover, no hypoxia-induced changes in RNA expression of canonical upstream regulators of this transcriptional complex in the Hippo pathway were observed, except for an increase in MST1 in MCF7 cells (Fig 2D).

Shared and distinct changes in expression of YAP/TAZ/TEAD target genes in response to hypoxia in luminal and basal A breast cancer cells

The response of three known YAP/TAZ target genes (CYR61, AXL, CTGF) to hypoxia in two luminal and two basal A TNBC cell lines showed an overall trend of increased expression in hypoxia, with CTGF being significantly enhanced in basal A but not luminal cells (Fig 2E). We next scrutinized hypoxia-regulated genes in MCF7 and HCC1143 cells identified by TempO-Seq for the presence of previously published YAP/TAZ target genes [36,37] (Fig 3A; Table S3). Most candidate targets found in MCF7 were also detected in HCC1143 (indicated in green). As an alternative approach, we analyzed hypoxia-regulated genes for enrichment of TEAD1-4 binding using DoRothEA [38] (Fig 3B; Table S4). Approximately half of the candidate TEAD binding genes found in MCF7 by this method were also detected in HCC1143 (indicated in blue). For both methods, the larger overall number of hypoxia-responsive genes identified in HCC1143 as compared to MCF7 (Table S2) was accompanied by a larger number of hypoxia-regulated candidate YAP/TAZ targets (Fig 3A, B). A small number of genes was identified by both methods, i.e., representing TEAD-binding, previously published YAP/TAZ target genes (Fig 3C). Of these, only WWC2, a WWC scaffolding protein involved in Hippo signaling [39] and ATAD2, an AAA+ ATPase and bromodomain family member with an as yet poorly understood oncogenic function [40], were shared between MCF7 and HCC1143 (Fig 3C). These findings show that while modulation of genes encoding elements of the Hippo pathway was not evident, overlapping as well as distinct sets of YAP/TAZ/TEAD target genes were modulated in luminal and basal A cells.

HIF1 mediated TAZ phosphorylation at Ser89 in basal A but not luminal breast cancer cells

YAP/TAZ/TEAD target genes may be modulated by hypoxia due to post-transcriptional regulation of YAP/TAZ in response to hypoxia. We therefore analyzed expression and phosphorylation of YAP/TAZ. In addition to specific YAP and TAZ antibodies, an antibody recognizing both p–YAP (Ser127) and p-TAZ (Ser89) was used, and signals were distinguished based on molecular weight. Total YAP and TAZ protein levels were not affected by hypoxia and phosphorylation of YAP at Ser127 in most of the cell lines, an event that is associated with cytoplasmic localization, 14-3-3 binding, and proteasomal degradation [32,41], showed no changes under hypoxia in any of the cell lines (Fig 4A). However, 3- and 5-days culture under hypoxia triggered a striking phosphorylation of TAZ at Ser89, similarly associated with cytoplasmic localization, 14-3-3 binding, and proteasomal degradation [42,43], in each of the basal A cell lines (Fig 4A). By contrast, none of the luminal breast cancer cells showed this response, with MCF7 displaying an opposite pattern with reduced p-TAZ (Ser89) under hypoxia. The basal A specific phosphorylation of TAZ at Ser89 under hypoxia was maintained for up to at least 10 days (Fig 4B). Moreover, the prominent difference between basal A and luminal cells with respect to hypoxia induced phosphorylation of TAZ at Ser89 was unaffected by

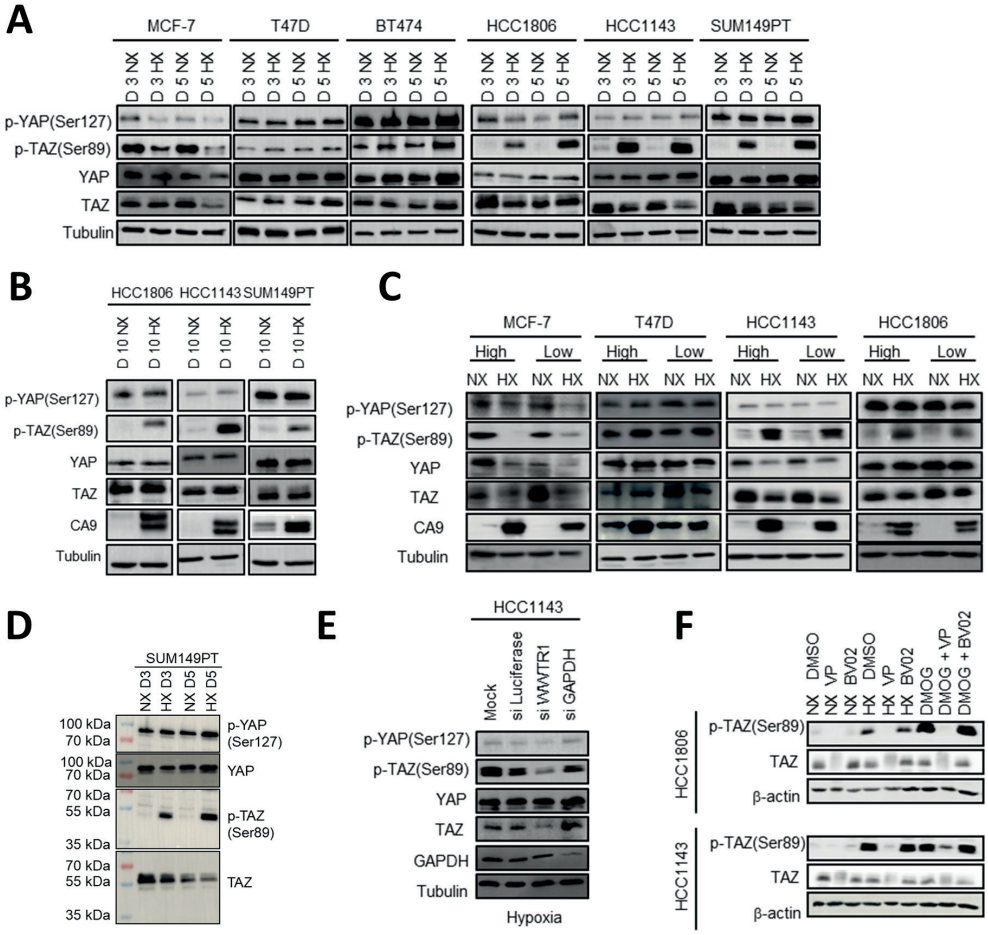

Figure 4. HIF1-mediated phosphorylation of TAZ at Ser89 under hypoxia in basal A but not luminal breast cancer cells. (A, B) Western blot showing YAP, TAZ, p-YAP (Ser127) and p-TAZ (Ser89) for three luminal (MCF7, T47D and BT474) and three basal A (SUM149PT, HCC1806 and HCC1143) breast cancer cell lines incubated under normoxia (NX) or hypoxia (HX) for 3 or 5 (A) or 10 days (B). Tubulin serves as loading control. **(C)** Western blot showing the indicated (phospho-)proteins for the indicated luminal and basal A cells seeded at low density (6 ×10^4 cells/petri dish; subconfluent) or high density (15°4 cells/petri dish; confluent) and exposed for 5 days to normoxia or hypoxia. **(D)** Western blot analysis of the indicated (phospho-)proteins for SUM149PT exposed for 3 or 5 days to normoxia or hypoxia. **(E)** Western blot analysis of the indicated (phospho-)proteins for HCC1143 cells treated with TAZ (WWTR1) SMARTpool siRNAs or the indicated control SMARTpool siRNAs and exposed for 5 days to hypoxia. **(F)** Western blot showing p-TAZ (Ser89) and TAZ in HCC1806 and HCC1143 cells cultured in absence or presence of Verteporfin (5μM) or BV02 (5μM) while exposed to normoxia, hypoxia, or DMOG (1mM) for 3 days. β-actin serves as loading control.

varying seeding densities, excluding differences in cell-cell contact area that are known to modulate YAP/TAZ [44–46] as the underlying mechanism (Fig 4C). p-TAZ (Ser89) showed a slightly lower molecular weight in the Western blot than total TAZ (Fig 4D).

To confirm specificity of the p-TAZ (Ser89) signal under hypoxia, WWTR1 silencing in HCC1143 using SMARTpool siRNA strongly reduced the p-TAZ (Ser89) signal as predicted while control luciferase and GAPDH siRNAs did not (Fig 4E). Phosphorylation of TAZ was also induced by treatment of HCC1143 and HCC1806 basal A cells with the HIF1α stabilizing compound DMOG under normoxic conditions, pointing to a HIF1 mediated response (Fig 4F). Treatment with Verteporfin, causing degradation of TAZ, also led to a corresponding loss of the p-TAZ (Ser89) signal induced by either hypoxia or DMOG, further confirming specificity. In these experiments, treatment with the 14-3-3 inhibitor BV02 did not affect total TAZ or p-TAZ (Ser89) levels in basal A cells under normoxic, hypoxic, or DMOG conditions. Together, these experiments point to a HIF1 mediated, basal A specific response to hypoxia by which TAZ, but not YAP, is phosphorylated at a site known to promote its cytoplasmic sequestration and proteasomal degradation [28,47] and which would consequently prevent TAZ from co-activating transcription of downstream target genes.

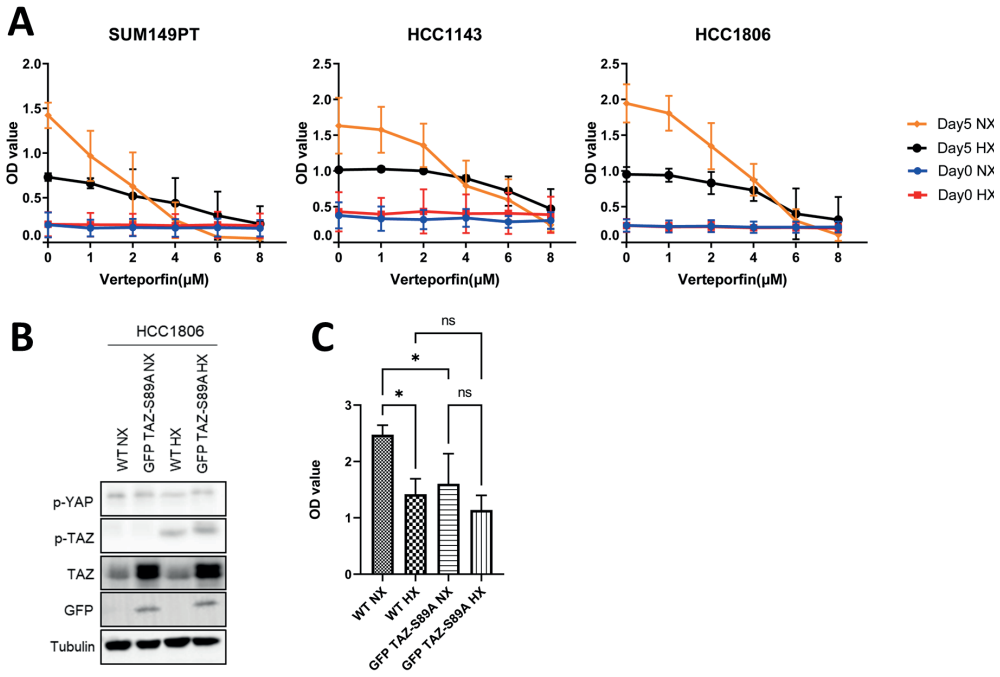

Figure 5. Effect of YAP/TAZ/TEAD complex inhibitor, Verteporfin and expression of GFP TAZ-S89A in basal A cells. (A) Results of SRB assay for three basal A breast cancer cell lines at day 0 (indicating equal cell seeding densities) and after 5 days incubation under normoxia or hypoxia in presence of 0 (DMSO vehicle control), 1, 2, 4, 6 or 8μM Verteporfin. Mean of raw OD values and SD for three biological replicates is shown. **(B, C)** GFP TAZ-S89A HCC1806 cells and wildtype HCC1806 cells (WT) were incubated under normoxia and hypoxia for 5 days and analyzed by Western blot (B) or SRB assay (C). For SRB assays, mean and SD of OD values from three biological replicates performed in triplicate are shown. ns, non-significant; *, $p<0.05$; ns, not significant.

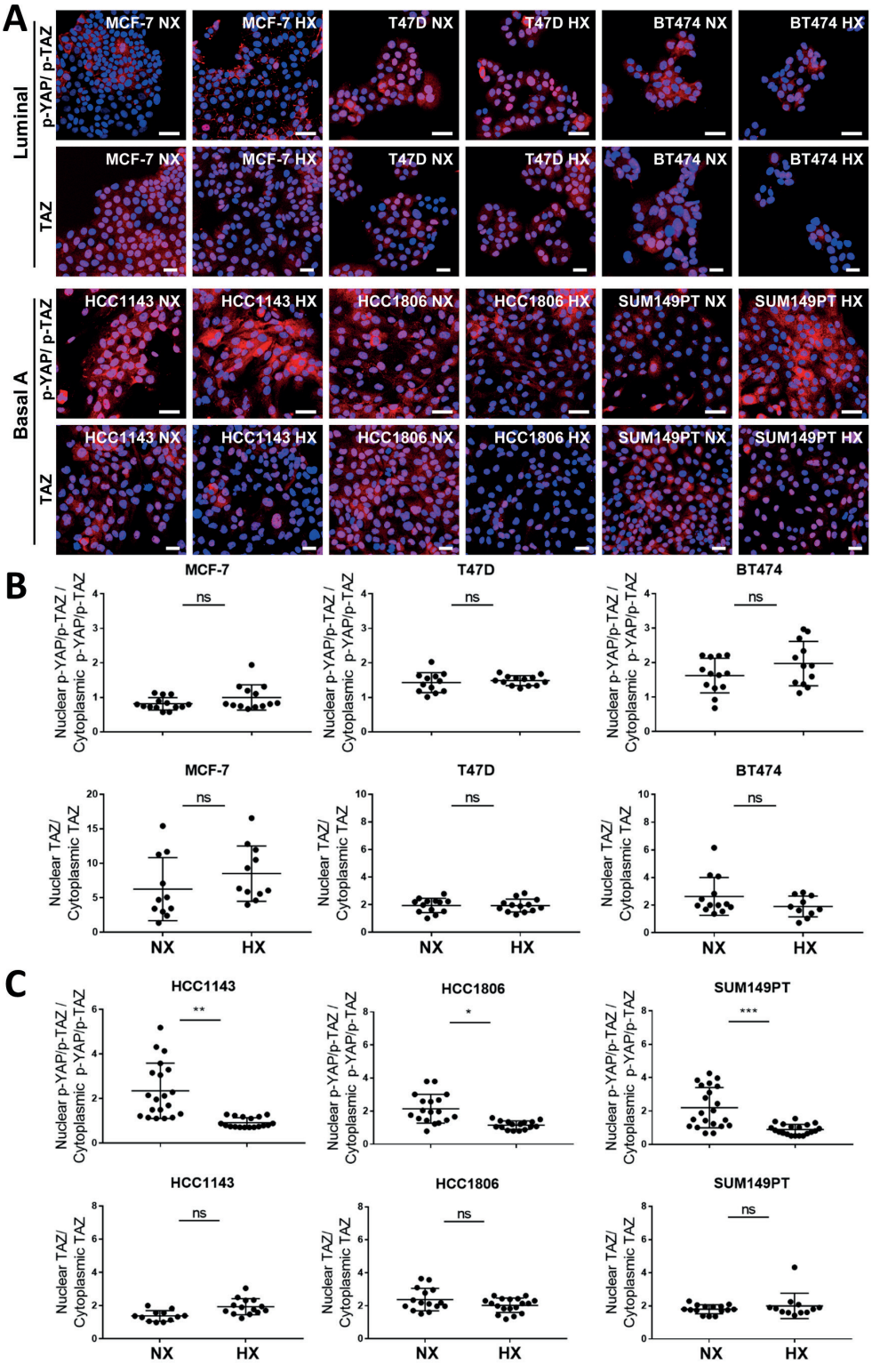
A
Luminal
p-YAP/ p-TAZ
TAZ
MCF-7 NX
MCF-7 HX
T47D NX
T47D HX
BT474 NX
BT474 HX
Basal A
HCC1143 NX
HCC1143 HX
HCC1806 NX
HCC1806 HX
SUM149PT NX
SUM149PT HX
B
MCF-7
T47D
BT474
Nuclear p-YAP/p-TAZ / Cytoplasmic p-YAP/p-TAZ
Nuclear TAZ/ Cytoplasmic TAZ
ns
NX
HX
C
HCC1143
HCC1806
SUM149PT
**
*
***

Figure 6. Localization of TAZ and phosphorylated YAP/TAZ in luminal breast cancer and basal A cells under normoxia and hypoxia. (A) Localization of TAZ and p-YAP/p-TAZ (using an Ab detecting both p-YAP (Ser127) and p-TAZ (Ser89)) determined by confocal immune fluorescence microscopy in luminal (MCF7, T47D and BT474) and basal A (SUM149PT, HCC1806 and HCC1143) breast cancer cell lines cultured under normoxia (NX) or hypoxia (HX) for 5 days. Blue, Hoechst; Red, Abs. **(B, C)** Quantification of nuclear/cytoplasmic distribution of TAZ and p-YAP/p-TAZ in luminal (B) and basal A cells (C) cultured under normoxia or hypoxia, calculated form images in (A). Y-axis indicates percentage of the total intensity in the nuclei area versus percentage of the total intensity in the cytoplasm area. *, $p < 0.05$; **, $p < 0.01$; ***, $p < 0.001$; ns, not significant.

Expression of a TAZ-S89A mutant does not prevent growth reduction in basal A cells under hypoxia

We wondered whether the increased TAZ phosphorylation under hypoxia was involved in the decreased growth of basal A cells under these conditions. Under hypoxia, growth of basal A cells was reduced and sensitivity to Verteporfin, a disruptor of YAP/TAZ-TEAD–mediated transcription decreased (Fig 5A). To assess if increased expression of unphosphorylated TAZ might confer basal A cells with a growth advantage under hypoxic conditions HCC1806 cells were transduced with a TAZ-S89A mutant. The expression of TAZ-S89A increased the total TAZ level, which, as expected, was not accompanied by enhanced levels of p-TAZ (Ser89) in normoxia or hypoxia (Fig 5B). However, the increased presence of non-phosphorylated TAZ did not confer basal A cells with a growth advantage under hypoxic conditions, indicating that other hypoxia/HIF regulated pathways suppressing cell growth were dominant (Fig 5C).

Basal A specific TAZ (Ser89) phosphorylation is accompanied by cytoplasmic localization in hypoxia

We next analyzed subcellular localization of YAP, TAZ, and phosphorylated YAP/TAZ in luminal and basal A cells under normoxia or hypoxia. TAZ was mostly concentrated in the nuclei of luminal as well as basal A cells and its localization appeared unaffected by hypoxia (Fig 6A-C). Likewise, YAP localization appeared largely nuclear in luminal and basal A cells and was unaffected by hypoxia (Fig S5, S6). Localization of [p-TAZ(Ser89)/ p-YAP(Ser127)] varied between luminal cell lines, appearing largely excluded from nuclei in MCF7 while being present in nuclei in T47D and BT474. This pattern was not affected under hypoxia. By contrast, localization of [p-TAZ(Ser89)/ p-YAP(Ser127)] under normoxia appeared largely nuclear in basal A cells (with some cytoplasmic signal in SUM149PT) and this switched to significantly more cytoplasmic staining under hypoxia in all basal A lines (Fig 6A, B). To specifically visualize localization of the increased levels of p-TAZ (Ser89) under hypoxic conditions in basal A cells, YAP knockout (KO) HCC1806 cells were generated. In the bulk KO population, most of the YAP signal disappeared (Fig 7A) and a corresponding increased nuclear concentration of TAZ was observed (Fig 7B). Under this condition most of the [p-TAZ(Ser89)/ p-YAP(Ser127)] signal disappeared indicating that the signal detected in WT cells was largely due to p-YAP (Ser127) rather than p-TAZ (Ser89) (Fig 7C). Further analysis of subcellular localization by cell fractionation confirmed an increase in nuclear total TAZ upon YAP KO and clearly showed that p-TAZ (Ser89) under hypoxic conditions in HCC1806 was largely localized in the cytoplasm (Fig 7D, E).

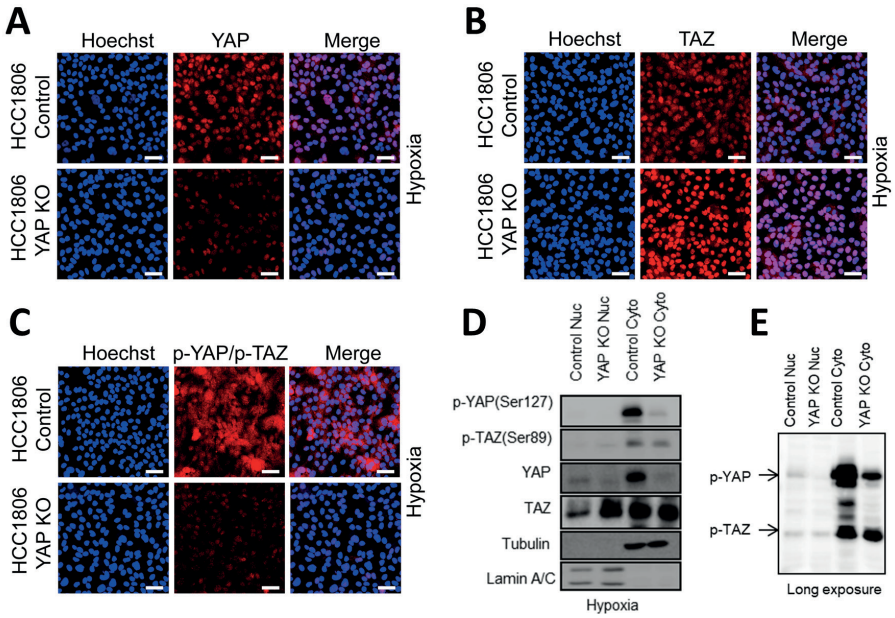

Figure 7. Subcellular localization of phospho-YAP/TAZ upon YAP knockout in HCC1806 cells under hypoxia. (A-C) YAP (A), TAZ (B) and phospho-YAP/TAZ (C) expression and localization analyzed by confocal immunofluorescence microscopy after 5-day incubation under hypoxia in CAS9 expressing HCC1806 cells transduced with YAP- or non-targeting control lentiviral sgRNA constructs. **(D)** Detection of YAP, TAZ, p-YAP (Ser127), and p-TAZ (Ser89) by Western blot after 5-day incubation under hypoxia in nuclear and cytoplasmic fractions of CAS9 expressing HCC1806 cells transduced with YAP- or non-targeting control lentiviral sgRNA constructs. Tubulin and Lamin A/C serve as loading controls for cytoplasmic and nuclear fraction, respectively **(E)** Longer exposure of Western blot used for (D).

Involvement of c-Src and CDK3 in TAZ Ser89 phosphorylation under hypoxia

We addressed which kinase could be responsible for phosphorylation of TAZ under hypoxia in basal A cells. No marked alterations in expression of kinases in the canonical upstream module of the Hippo pathway were identified in basal A under hypoxia (Fig 2D) and silencing of MST1, LATS1, or LATS2 did not affect hypoxia induced TAZ Ser89 phosphorylation in HCC1143 cells (Fig 8A). Src activity has been implicated in the upstream regulation of YAP/TAZ/TEAD transcriptional activity in different biological settings [48–56]. We observed a marked inhibition of hypoxia induced p-TAZ (Ser89) upon exposure to the Src inhibitor PP2 in three basal A cell lines, but p-Src (Y416) was only weakly affected (Fig 8B). By contrast, PP2 did not inhibit p-TAZ (Ser89) in luminal cells under normoxic or hypoxic conditions (Fig 8C). Another Src inhibitor, Dasatinib also reduced p-TAZ (Ser89) in HCC1143 basal A cells under hypoxia and this compound did reduce p-Src (Y416) levels as expected (Fig 8D). Together, these results suggested that the tyrosine kinase Src was involved in hypoxia induced TAZ (Ser89) phosphorylation in basal A cells but also pointed to an off-target effect of PP2 based on its weak effect on p-Src (Y416) levels. From a series of ChEMBL predicted PP2 targets, the serine/threonine-protein kinase CDK3 stood out in the top 10 as it scored much lower for predicted activity to interact with Dasatinib (Fig 8E; Table S1). Silencing CDK3 in HCC1143

cells using an siRNA SMARTpool as well as expression of CDK3 shRNAs, significantly reduced p-TAZ (Ser89) in these basal A cells under hypoxia (Fig 8F, G). Together, these results indicated that hypoxia/HIF1 mediated TAZ Ser89 phosphorylation is supported by the activity of c-Src and involves an off target PP2 substrate, identified as CDK3.

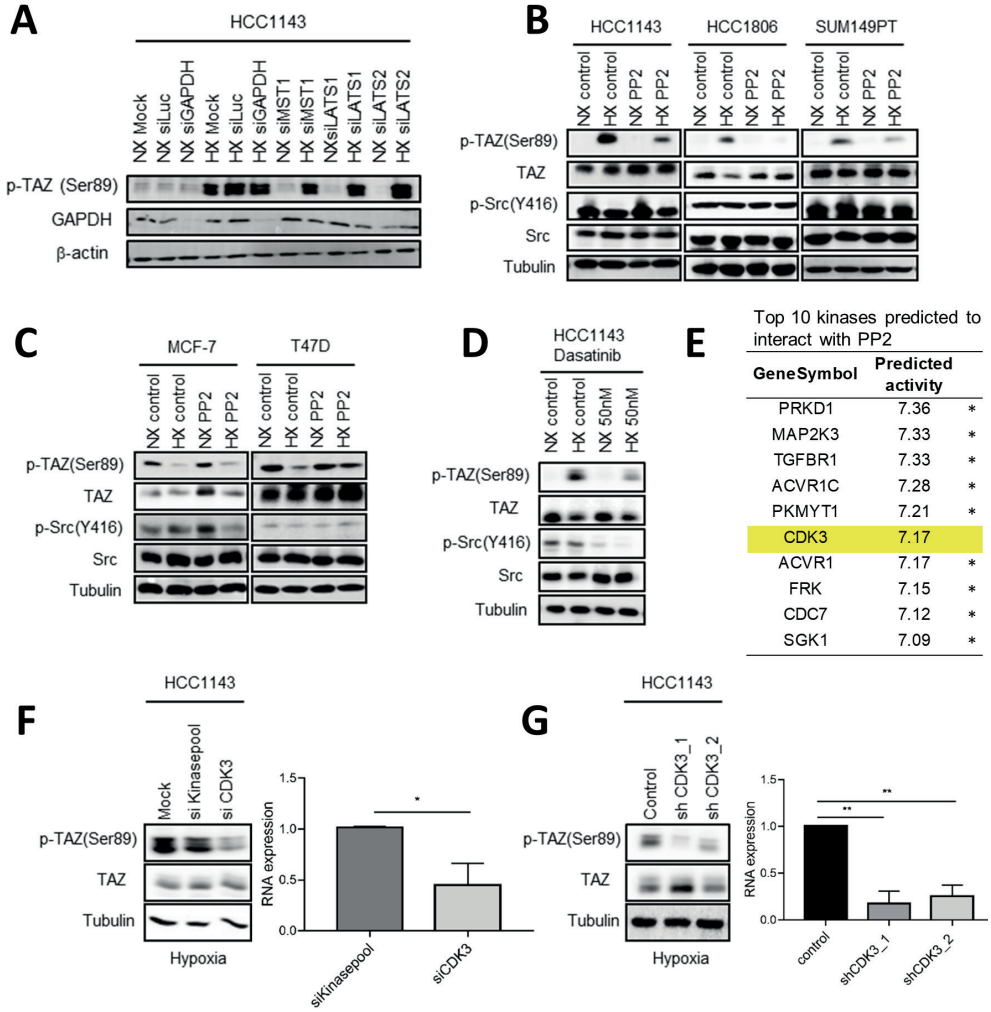

Figure 8. Src and CDK3 mediate phosphorylation of TAZ on Ser89 under hypoxia in basal A cells. (A) Western blot analysis of p-TAZ (Ser89) in HCC1143 cells treated with the indicated SMARTpool siRNAs targeting components of the Hippo signaling cascade or luciferase or GAPDH as controls and exposed for 5 days to normoxia (NX) or hypoxia (HX). β-actin serves as loading control. **(B, C)** Western blot analysis of the indicated (phospho-)proteins in the indicated basal A (B) or luminal breast cancer cell lines (C) exposed to normoxia or hypoxia for 3 days in absence or presence of 1μM PP2. Tubulin serves as loading control. **(D)** Western blot analysis of the indicated (phospho-)proteins in HCC1143 basal A cells exposed to normoxia or hypoxia for 3 days in absence or presence of 50nM Dasatinib. **(E)** Top 10 kinases identified as candidate PP2 substrates by ChEMBL ranked by activity. *Indicates kinases where interaction with Dasatinib scored higher interaction with PP2. **(F, G)** Western blot analysis of TAZ and p-TAZ (Ser89) in HCC1143 cells treated with control (kinase pool) or CDK3 targeting SMARTpool

siRNAs (F) or in HCC1143 cells transduced with control non-targeting or 2 different CDK3 targeting lentiviral shRNA constructs (G). Cells were exposed for 5 days to hypoxia. Graphs show qPCR analysis of gene silencing efficacy of the CDK3 targeting siRNA SMARTpool (F) or the CDK3 targeting lentiviral shRNA constructs (G). Mean expression relative to β-actin is shown. Error bars indicate SD for triplicate measurements. *, $p<0.05$; **, $p<0.01$.

Discussion

In this work, we explore hypoxia regulated changes in gene expression in luminal breast cancer versus basal A TNBC cells and focus on YAP/TAZ signaling. We show that HIF stabilization and expression of a key HIF target, CA9 are similarly induced in response to hypoxia in both breast cancer subtypes. Despite conservation of the canonical HIF-mediated response to hypoxia, the impact of hypoxia on genome wide gene expression differs between luminal and basal A cells. The response to hypoxia for YAP/TAZ target genes, identified based on existing literature as well as predicted to harbor TEAD binding sites is limited. Notably, prediction of enhanced YAP/TAZ activity based on changes in target gene expression is hampered by the fact that other transcription factors are involved as well, including for instance cross talk between YAP/TAZ-TEAD and MRTF–SRF transcriptional complexes in gene regulation [25,57].

Our analyses showing that TAZ, and to a lesser extent YAP RNA levels are higher in basal-like breast cancer cell lines and in TNBC patients as compared to luminal breast cancer cell lines and ER positive patients, respectively agree with earlier work. TAZ protein expression has been reported to increase from barely detectable in low-grade invasive ductal breast carcinomas to strong nuclear staining in ~80% of high-grade invasive ductal breast carcinomas [58]. Studies have associated TAZ expression levels with the TNBC subtype and amplification of the WWTR gene can explain only a fraction of the overexpression cases indicating that other mechanisms must be at play (reviewed in [59]). TAZ may be involved in the increased aggressiveness of TNBC by promoting breast cancer stem cell self-renewal and tumor initiation capacity [58,59].

We reveal a HIF1 mediated response to hypoxia occurring in all basal A TNBC cells tested, but not in any of the luminal breast cancer lines, which leads to phosphorylation of TAZ at a site known to suppress nuclear localization and transcriptional activity. This striking response is not affected by cell density, which has a major influence of YAP/TAZ activity [44–46]. Similar findings have been reported for ovarian breast cancer cells indicating that this response may be conserved among distinct cancer types and, in agreement with our study, the Hippo pathway kinase Lats1 was not involved [28]. Our results do not corroborate an earlier report showing that HIF-1 transcriptionally activates the WWTR gene in breast cancer cells [29,30]. No increase in total TAZ levels nor TAZ nuclear accumulation is observed by us upon switching any of the cell lines from normoxia to hypoxia.

We show that hypoxia-induced phosphorylation of TAZ at Ser89 in basal A TNBC cells is not mediated by the canonical Hippo kinases [25,26]. Rather, our results indicate that c-Src supports this event and an off target of the PP2 Src inhibitor, CDK3 is involved. Src family kinases have been previously implicated in phosphorylation of YAP but in that case considered as positive regulators of YAP activity [60,61]. We find that the phosphorylation

of TAZ at Ser89 in hypoxic basal A TNBC cells is accompanied by an increase in cytoplasmic localization suggesting that in this case activity of TAZ is attenuated. Interestingly, recent work by others has shown that CDK7 can phosphorylate YAP, but in that case, it involves an activating phosphorylation at Ser128 (adjacent to the inactivating phosphorylation site, Ser127) that protects YAP from ubiquitination [62]. Interactions of CDKs with TAZ have not been previously described. Notably, the dominance of YAP phosphorylation (revealed in our experiments by the major loss of [p-TAZ(Ser89)/ p-YAP(Ser127)] upon deletion of YAP), likely masks functional consequences of TAZ Ser89 phosphorylation for cell survival and proliferation in basal A TNBC cells under hypoxia.

In conclusion, we find that even though HIF1α stabilization is activated similarly in basal and luminal breast cancer cells the response to hypoxia differs with distinct patterns of gene regulation. HIF1 mediated phosphorylation of TAZ, but not YAP, at a site known to promote its cytoplasmic sequestration and proteasomal degradation, is observed in basal A but not luminal cells. We show that Src and CDK3 are implicated in this response. Further studies investigating the mechanism and functional consequence of such modulation of TAZ are warranted.

Supplementary Materials:
The following supporting information can be downloaded at: https://www.mdpi.com/article/10.3390/ijms231710119/s1.

Author Contributions:
Q.L., S.E.L.D., E.H.J.D. conceived the study. Q.L. performed the experiments with assistance of V.E.v.d.N., H.L., B.C., K.E., J.T.M.P. W.v.d.S. O.J.M.B., G.v.W. contributed the kinase-substrate predictions. Q.L., S.E.L.D., E.H.J.D. wrote the paper with input from all authors. All authors have read and agreed to the published version of the manuscript.

Funding:
QL was supported by a grant from the China Scholarship Council (201706550007). BC was supported by the Dutch Cancer Society (KWF Research Grant #10967).

Data Availability Statement:
TempO-Seq data supporting the results of this article will be avail-able in the BioStudies database from EMBL-EBI.

Acknowledgments:
The authors thank Hans de Bont and Annaloes Fokkelman Klip from LACDR at Leiden University for technical assistance with microscopy and plasmid sequencing; Gangyin Zhao and Ewa Snaar Jagalska from IBL at Leiden University for the lenti-TAZ-S89A-IRES-GFP construct; and Sylvestre Bonnet and Xuequan Zhou from LIC at Leiden University for sharing the hypoxia incubator and cell fractionation reagents.

Conflicts of Interest:
The authors declare that they have no competing interests.

References
1.Anderson, W. F., Rosenberg, P. S., Prat, A., Perou, C. M. & Sherman, M. E. How many etiological subtypes of breast cancer: two, three, four, or more? Journal of the National Cancer Institute 106 (2014).
2.Ahn, H. J., Jung, S. J., Kim, T. H., Oh, M. K. & Yoon, H.-K. Differences in Clinical Outcomes between Luminal A and B Type Breast Cancers according to the St. Gallen Consensus 2013. Journal of breast cancer 18, 149–159 (2015).
3.Creighton, C. J. The molecular profile of luminal B breast cancer. Biologics : targets & therapy 6, 289–297 (2012).
4.Perou, C. M. et al. Molecular portraits of human breast tumours. Nature 406, 747–752 (2000).
5.Sorlie, T. et al. Repeated observation of breast tumor subtypes in independent gene expression data sets. Proceedings of the National Academy of Sciences of the United States of America 100, 8418–8423 (2003).
6.Badve, S. et al. Basal-like and triple-negative breast cancers: a critical review with an emphasis on the implications for pathologists and oncologists. Modern pathology : an official journal of the United States and Canadian Academy of Pathology, Inc 24, 157–167 (2011).
7.Anders, C. & Carey, L. A. Understanding and treating triple-negative breast cancer. Oncology (Williston Park, N.Y.) 22, 1233-9; discussion 1239-40, 1243 (2008).
8.Fulford, L. G. et al. Basal-like grade III invasive ductal carcinoma of the breast: patterns of metastasis and long-term survival. Breast cancer research : BCR 9, R4 (2007).
9.Yao, H. et al. Triple-negative breast cancer: is there a treatment on the horizon? Oncotarget 8, 1913–1924 (2017).
10.Coban, B., Bergonzini, C., Zweemer, A. J. M. & Danen, E. H. J. Metastasis: crosstalk between tissue mechanics and tumour cell plasticity. British journal of cancer 124, 49–57 (2021).
11.Hanahan, D. & Weinberg, R. A. Hallmarks of cancer: the next generation. Cell 144, 646–674 (2011).
12.LaGory, E. L. & Giaccia, A. J. The ever-expanding role of HIF in tumour and stromal biology. Nature cell biology 18, 356–365 (2016).
13.Semenza, G. L. Molecular mechanisms mediating metastasis of hypoxic breast cancer cells. Trends in molecular medicine 18, 534–543 (2012).
14.Folkman, J. Role of angiogenesis in tumor growth and metastasis. Seminars in oncology 29, 15–18 (2002).
15.Parks, S. K., Cormerais, Y. & Pouysségur, J. Hypoxia and cellular metabolism in tumour pathophysiology. The Journal of physiology 595, 2439–2450 (2017).
16.Vaupel, P. & Mayer, A. Hypoxia in cancer: significance and impact on clinical outcome. Cancer metastasis reviews 26, 225–239 (2007).
17.Huang, L. E., Gu, J., Schau, M. & Bunn, H. F. Regulation of hypoxia-inducible factor 1alpha is mediated by an O2-dependent degradation domain via the ubiquitin-proteasome pathway. Proceedings of the National Academy of Sciences of the United States of America 95, 7987–7992 (1998).
18.Wang, G. L., Jiang, B. H., Rue, E. A. & Semenza, G. L. Hypoxia-inducible factor 1 is a basic-helix-loop-helix-PAS heterodimer regulated by cellular O2 tension. Proceedings of the National Academy of Sciences of the United States of America 92, 5510–5514 (1995).
19.Vaupel, P., Höckel, M. & Mayer, A. Detection and characterization of tumor hypoxia using pO2 histography. Antioxidants & redox signaling 9, 1221–1235 (2007).
20.Bos, R. et al. Levels of hypoxia-inducible factor-1alpha independently predict prognosis in patients with lymph node negative breast carcinoma. Cancer 97, 1573–1581 (2003).
21.Dales, J.-P. et al. Overexpression of hypoxia-inducible factor HIF-1alpha predicts early relapse in breast cancer: retrospective study in a series of 745 patients. International journal of cancer 116, 734–739 (2005).
22.Generali, D. et al. Hypoxia-inducible factor-1alpha expression predicts a poor response to primary chemoendocrine therapy and disease-free survival in primary human breast cancer. Clinical cancer research : an official journal of the American Association for Cancer Research 12, 4562–4568 (2006).
23.Giatromanolaki, A. et al. c-erbB-2 related aggressiveness in breast cancer is hypoxia inducible factor-1alpha dependent. Clinical cancer research : an official journal of the American Association for Cancer Research 10, 7972–7977 (2004).
24.Schindl, M. et al. Overexpression of hypoxia-inducible factor 1alpha is associated with an unfavorable prognosis in lymph node-positive breast cancer. Clinical cancer research : an official journal of the American Association for Cancer Research 8, 1831–1837 (2002).
25.Pocaterra, A., Romani, P. & Dupont, S. YAP/TAZ functions and their regulation at a glance. Journal of cell science 133 (2020).
26.Piccolo, S., Dupont, S. & Cordenonsi, M. The biology of YAP/TAZ: hippo signaling and beyond. Physiological reviews 94, 1287–1312 (2014).
27.Preisser, F., Giehl, K., Rehm, M. & Goppelt-Struebe, M. Inhibitors of oxygen sensing prolyl hydroxylases regulate nuclear localization of the transcription factors Smad2 and YAP/TAZ involved in CTGF synthesis. Biochimica et biophysica acta 1863, 2027–2036 (2016).
28.Yan, L., Cai, Q. & Xu, Y. Hypoxic conditions differentially regulate TAZ and YAP in cancer cells. Archives of biochemistry and biophysics 562, 31–36 (2014).
29.Xiang, L. et al. Hypoxia-inducible factor 1 mediates TAZ expression and nuclear localization to induce the breast cancer stem cell phenotype. Oncotarget 5, 12509–12527 (2014).
30.Xiang, L. et al. HIF-1α and TAZ serve as reciprocal co-activators in human breast cancer cells. Oncotarget 6, 11768–11778 (2015).
31.Yeakley, J. M. et al. A trichostatin A expression signature identified by TempO-Seq targeted whole transcriptome profiling. PloS one 12, e0178302 (2017).
32.Kim, M.-K., Jang, J.-W. & Bae, S.-C. DNA binding partners of YAP/TAZ. BMB reports 51, 126–133 (2018).
33.Zanconato, F. et al. Genome-wide association between YAP/TAZ/TEAD and AP-1 at enhancers drives oncogenic growth. Nature cell biology 17, 1218–1227 (2015).
34.Garcia-Alonso, L. et al. Transcription Factor Activities Enhance Markers of Drug Sensitivity in Cancer. Cancer research 78, 769–780 (2018).
35.van der Stel, W. et al. Mapping the cellular response to electron transport chain inhibitors reveals selective signaling networks triggered by mitochondrial perturbation. Archives of toxicology 96, 259–285 (2022).
36.Alvarez, M. J. et al. Functional characterization of somatic mutations in cancer using network-based inference of protein activity. Nature genetics 48, 838–847 (2016).
37.Koedoot, E. et al. Differential reprogramming of breast cancer subtypes in 3D cultures and implications for sensitivity to targeted therapy. Scientific reports 11, 7259 (2021).
38.Zhu, Y., Qiu, P. & Ji, Y. TCGA-assembler: open-source software for retrieving and processing TCGA data. Nature methods 11, 599–600 (2014).
39.Koedoot, E. et al. Co-regulated gene expression of splicing factors as drivers of cancer progression. Scientific reports 9, 5484 (2019).
40.Hoadley, K. A. et al. Cell-of-Origin Patterns Dominate the Molecular Classification of 10,000 Tumors from 33 Types of Cancer. Cell 173, 291-304.e6 (2018).
41.Cerami, E. et al. The cBio cancer genomics portal: an open platform for exploring multidimensional cancer genomics data. Cancer discovery 2, 401–404 (2012).
42.Zhou, Y. et al. Metascape provides a biologist-oriented resource for the analysis of systems-level datasets. Nature communications 10, 1523 (2019).
43.Gaulton, A. et al. The ChEMBL database in 2017. Nucleic acids research 45, D945-D954 (2017).

44.Sjöström, M., Rännar, S. & Wieslander, Å. Polypeptide sequence property relationships in Escherichia coli based on auto cross covariances. Chemometrics and Intelligent Laboratory Systems 29, 295–305 (1995).
45.Lenselink, E. B. et al. Beyond the hype: deep neural networks outperform established methods using a ChEMBL bioactivity benchmark set. Journal of cheminformatics 9, 45 (2017).
46.Georgiev, A. G. Interpretable numerical descriptors of amino acid space. Journal of computational biology : a journal of computational molecular cell biology 16, 703–723 (2009).
47.van Westen, G. J. et al. Benchmarking of protein descriptor sets in proteochemometric modeling (part 1): comparative study of 13 amino acid descriptor sets. Journal of cheminformatics 5, 41 (2013).
48.Zhou, P. et al. A new descriptor of amino acids based on the three-dimensional vector of atomic interaction field. CHINESE SCI BULL 51, 524–529 (2006).
49.Hellberg, S., Sjöström, M., Skagerberg, B. & Wold, S. Peptide quantitative structure-activity relationships, a multivariate approach. Journal of medicinal chemistry 30, 1126–1135 (1987).
50.Chen, T. & Guestrin, C. In Proceedings of the 22nd ACM SIGKDD International Conference on Knowledge Discovery and Data Mining, edited by B. Krishnapuram, et al. (ACM, 08132016), pp. 785–794.
51.Qiu, G.-Z. et al. Reprogramming of the Tumor in the Hypoxic Niche: The Emerging Concept and Associated Therapeutic Strategies. Trends in pharmacological sciences 38, 669–686 (2017).
52.Zhao, C. et al. Yes-associated protein (YAP) and transcriptional coactivator with a PDZ-binding motif (TAZ): a nexus between hypoxia and cancer. Acta pharmaceutica Sinica. B 10, 947–960 (2020).
53.Comprehensive molecular portraits of human breast tumours. Nature 490, 61–70 (2012).
54.Ciriello, G. et al. Comprehensive Molecular Portraits of Invasive Lobular Breast Cancer. Cell 163, 506–519 (2015).
55.Garcia-Alonso, L., Holland, C. H., Ibrahim, M. M., Turei, D. & Saez-Rodriguez, J. Benchmark and integration of resources for the estimation of human transcription factor activities. Genome research 29, 1363–1375 (2019).
56.Höffken, V., Hermann, A., Pavenstädt, H. & Kremerskothen, J. WWC Proteins: Important Regulators of Hippo Signaling in Cancer. Cancers 13 (2021).
57.Nayak, A., Dutta, M. & Roychowdhury, A. Emerging oncogene ATAD2: Signaling cascades and therapeutic initiatives. Life sciences 276, 119322 (2021).
58.Liu, H. et al. Multifaceted regulation and functions of YAP/TAZ in tumors (Review). Oncology reports 40, 16–28 (2018).
59.Kim, Y. & Jho, E.-H. Regulation of the Hippo signaling pathway by ubiquitin modification. BMB reports 51, 143–150 (2018).
60.Kanai, F. et al. TAZ: a novel transcriptional co-activator regulated by interactions with 14-3-3 and PDZ domain proteins. The EMBO journal 19, 6778–6791 (2000).
61.Zhang, Q. et al. Yes-associated protein (YAP) and transcriptional coactivator with PDZ-binding motif (TAZ) mediate cell density-dependent proinflammatory responses. The Journal of biological chemistry 293, 18071–18085 (2018).
62.Zhao, B. et al. Inactivation of YAP oncoprotein by the Hippo pathway is involved in cell contact inhibition and tissue growth control. Genes & development 21, 2747–2761 (2007).
63.Furukawa, K. T., Yamashita, K., Sakurai, N. & Ohno, S. The Epithelial Circumferential Actin Belt Regulates YAP/TAZ through Nucleocytoplasmic Shuttling of Merlin. Cell reports 20, 1435–1447 (2017).
64.Chen, Y.-A. et al. WW Domain-Containing Proteins YAP and TAZ in the Hippo Pathway as Key Regulators in Stemness Maintenance, Tissue Homeostasis, and Tumorigenesis. Frontiers in oncology 9, 60 (2019).
65.Anwar, T., Sinnett-Smith, J., Jin, Y.-P., Reed, E. F. & Rozengurt, E. Ligation of HLA Class I Molecules Induces YAP Activation through Src in Human Endothelial Cells. Journal of immunology (Baltimore, Md. : 1950) 205, 1953–1961 (2020).
66.Byun, M. R. et al. SRC activates TAZ for intestinal tumorigenesis and regeneration. Cancer letters 410, 32–40 (2017).
67.Guillermin, O. et al. Wnt and Src signals converge on YAP-TEAD to drive intestinal regeneration. The EMBO journal 40, e105770 (2021).
68.Kim, J. et al. Proline-rich tyrosine kinase 2 mediates transforming growth factor-beta-induced hepatic stellate cell activation and liver fibrosis. Scientific reports 10, 21018 (2020).
69.Kim, N.-G. & Gumbiner, B. M. Adhesion to fibronectin regulates Hippo signaling via the FAK-Src-PI3K pathway. The Journal of cell biology 210, 503–515 (2015).
70.Lamar, J. M. et al. SRC tyrosine kinase activates the YAP/TAZ axis and thereby drives tumor growth and metastasis. The Journal of biological chemistry 294, 2302–2317 (2019).
71.Ma, H. et al. Periostin Promotes Colorectal Tumorigenesis through Integrin-FAK-Src Pathway-Mediated YAP/TAZ Activation. Cell reports 30, 793-806.e6 (2020).
72.Shanzer, M., Adler, J., Ricardo-Lax, I., Reuven, N. & Shaul, Y. The nonreceptor tyrosine kinase c-Src attenuates SCF(β-TrCP) E3-ligase activity abrogating Taz proteasomal degradation. Proceedings of the National Academy of Sciences of the United States of America 114, 1678–1683 (2017).
73.Yui, S. et al. YAP/TAZ-Dependent Reprogramming of Colonic Epithelium Links ECM Remodeling to Tissue Regeneration. Cell stem cell 22, 35-49.e7 (2018).
74.Foster, C. T., Gualdrini, F. & Treisman, R. Mutual dependence of the MRTF-SRF and YAP-TEAD pathways in cancer-associated fibroblasts is indirect and mediated by cytoskeletal dynamics. Genes & development 31, 2361–2375 (2017).
75.Cordenonsi, M. et al. The Hippo transducer TAZ confers cancer stem cell-related traits on breast cancer cells. Cell 147, 759–772 (2011).
76.Fresques, T. & LaBarge, M. A. <PE-ATContributions of Yap and Taz dysfunction to breast cancer initiation, progression, and aging-related susceptibility. Aging and cancer 1, 5–18 (2020).
77.Tamm, C., Böwer, N. & Annerén, C. Regulation of mouse embryonic stem cell self-renewal by a Yes-YAP-TEAD2 signaling pathway downstream of LIF. Journal of cell science 124, 1136–1144 (2011).
78.Rosenbluh, J. et al. β-Catenin-driven cancers require a YAP1 transcriptional complex for survival and tumorigenesis. Cell 151, 1457–1473 (2012).
79.Cho, Y. S. et al. CDK7 regulates organ size and tumor growth by safeguarding the Hippo pathway effector Yki/Yap/Taz in the nucleus. Genes & development 34, 53–71 (2020).

Supplemental data

Table S1. Kinase-substrate predictions of PP2 and Dasatinib based on activity values of human kinase proteins collected from ChEMBL. Lists showing description of molecular descriptors, predicted activity of Dasatinib, and predicted activity of PP2.

Table S1: List of molecular descriptors		Table S1: Model based only on kinase substrates (data from ChEMBL) of Dasatinib				Table S1: Model based only on kinase substrates (data from ChEMBL) of PP2			
descriptor	description	hgnc_id	gene symbol	accession	pred_activity	hgnc_id	gene symbol	accession	pred_activity
Molecular_SASA	2D approximated solvent accessible surface area	19310	PIM3	Q86V86	8.91	9407	PRKD1	Q15139	7.36
ALogP	octanol-water partition coefficient	8986	PIM1	P11309	8.76	6843	MAP2K3	P46734	7.33
OtherAtom_fraction	being F, Cl, I, Br, S, O, N, H or C	6843	MAP2K3	P46734	8.51	11772	TGFBR1	P36897	7.33
Carbon_fraction	Fraction of carbon atoms	12440	TYK2	P29597	8.43	18123	ACVR1C	Q8NER5	7.28
Halogen_fraction	Fraction of halogen atoms	12440	TYK2	P29597	8.43	29650	PKMYT1	Q99640	7.21
Heteroatom_fraction	Fraction of hetero atoms	9407	PRKD1	Q15139	8.42	1772	CDK3	Q00526	7.17
Hydrogen_fraction	Fraction of hydrogen atoms	6190	JAK1	P23458	8.42	171	ACVR1	Q04771	7.17
H_Acceptors_Fraction	Fraction of hydrogen bond acceptors	6190	JAK1	P23458	8.42	3955	FRK	P42685	7.15
H_Donors_fraction	Fraction of hydrogen bond donors	7110	MKNK1	Q9BUB5	8.41	1745	CDC7	O00311	7.12
Molecular_PolarSASA_Fraction	Fraction of molecular polar surface area	1462	CAMK2D	Q13557	8.34	10810	SGK1	O00141	7.09
NegativeAtom_Fraction	Fraction of negatively charged atoms	6192	JAK2	O60674	8.27	6875	MAPK13	O15264	7.09
Nitrogen_fraction	Fraction of nitrogen atoms	6192	JAK2	O60674	8.27	16835	TAOK2	Q9UL54	7.07
Oxygen_fraction	Fraction of oxygen atoms	9393	PRKCA	P17252	8.26	7111	MKNK2	Q9HBH9	7.07
Phosphorus_fraction	Fraction of phosphorus atoms	8987	PIM2	Q9P1W9	8.24	6855	MAP3K3	Q99759	7.06
Molecular_PolarSurface Area_Fraction	Fraction of polar surface area	6850	MAP3K11	Q16584	8.24	7748	NEK5	Q6P3R8	7.02
PositiveAtom_Fraction	Fraction of positively charged atoms	10434	RPS6KA5	O75582	8.23	19310	PIM3	Q86V86	7.02
…	…	…	…	…	…	…	…	…	…
…	…	…	…	…	…	…	…	…	…

Table S2. Hypoxia induced DEGs in MCF7 and HCC1143. Lists of DEGs derived from TempO-Seq analysis of MCF7 and HCC1143 cells exposed to 5-day hypoxia relative to normoxia using a cutoff of [|Log_2Foldchange|>1; padj<0.05].

Table S2: Hypoxia induced DEGs in MCF7									
baseMean	log2FoldChange	lfcSE	stat	pvalue	padj	Probe_ID	GeneSymbol	ProbeNr	Entrez_ID
147.814889	-1.1808668	0.451307327	-2.616546931	0.008882415	0.049915705	CHCHD10_21375	CHCHD10	21375	400916
31.02073507	-1.717010317	0.65558796	-2.619038821	0.008817791	0.049633313	POLDIP2_5246	POLDIP2	5246	26073
24.31721814	1.571670993	0.599151582	2.623160881	0.008711812	0.049197165	SDK1_23081	SDK1	23081	221935
111.7099141	1.065510532	0.40614482	2.623474385	0.008703799	0.049172014	MFSD1_92612	MFSD1	92612	64747
57.68673769	1.10178434	0.419915707	2.623822643	0.008694905	0.049161982	RPL13_92993	RPL13	92993	6137
…	…	…	…	…	…	…	…	…	…
…	…	…	…	…	…	…	…	…	…
Table S2: Hypoxia induced DEGs in HCC1143									
baseMean	log2FoldChange	lfcSE	stat	pvalue	padj	Probe_ID	GeneSymbol	ProbeNr	Entrez_ID
29.20300377	-3.932217274	1.155328567	-3.4035489	0.000665165	0.002522011	CHAC1_1279	CHAC1	1279	79094
63.76323051	-1.754480777	0.561341742	-3.125512758	0.001774954	0.005969128	AKAP8L_196	AKAP8L	196	26993
22.08528186	1.916520888	0.8017014	2.390566971	0.016822381	0.04176531	IGFBP4_3271	IGFBP4	3271	3487
148.2262154	-1.683627611	0.534501897	-3.149900162	0.001633263	0.005562926	STIP1_6841	STIP1	6841	10963
…	…	…	…	…	…	…	…	…	…
…	…	…	…	…	…	…	…	…	…

Table S3. Published YAP TAZ target genes. A list of YAP and/or TAZ target genes previously identified [32,33].

Table S3. Published YAP TAZ target genes			
ABHD10	ARSJ	BTBD10	CTNNAL1
ACAT2	ASAP1	BUB1B	CUTC
ADAMTS16	ASB1	C11orf48	CYC1
ADAMTS6	ATAD2	C11orf83	CYP20A1
ADRB2	ATG3	C12orf45	CYR61
AFAP1L1	AXL	C12orf65	DARS2
AIMP2	B3GALNT2	C17orf89	DDAH1
AJUBA	BANF1	C1orf109	DDX21
AKAP12	BASP1	C1QBP	DDX46
AMOTL2	BCAT1	C4BPB	DDX47
ANKRD1	BCS1L	C5orf28	DDX56
...	...	...	...
...	...	...	...

Table S4. TEAD1-4 binding genes identified by DoRothEA in all genes in the TempO-Seq whole genome library. A list of TEAD1-4 binding genes identified by transcription factor enrichment analysis using the DoRothEA tool with log2 normalized values for the TempO-Seq data.

Table S4. TEAD1-4 binding genes identified by DoRothEA in all genes in the TempoSeq whole genome library					
Targets	**TF**	**Targets**	**TF**	**Targets**	**TF**
ABCA4	TEAD1	ALDH1A1	TEAD1	CCDC171	TEAD1
ABLIM3	TEAD1	AMIGO2	TEAD1	CCDC80	TEAD1
AC002066.1	TEAD1	AMOTL2	TEAD1	CDH18	TEAD1
AC003984.1	TEAD1	ANGPT1	TEAD1	CDH2	TEAD1
AC005062.2	TEAD1	ANKFN1	TEAD1	CFL1P3	TEAD1
AC006076.1	TEAD1	ANO6	TEAD1	CHN1	TEAD1
AC006369.2	TEAD1	ANXA1	TEAD1	CLIC5	TEAD1
AC011286.1	TEAD1	ANXA3	TEAD1	CLIP4	TEAD1
AC058791.1	TEAD1	ANXA5	TEAD1	CNOT1	TEAD1
AC068138.1	TEAD1	ARHGAP18	TEAD1	COL11A1	TEAD1
AC073130.3	TEAD1	ARHGAP29	TEAD1	COL8A1	TEAD1
...	...	...	...	...	...
...	...	...	...	...	...

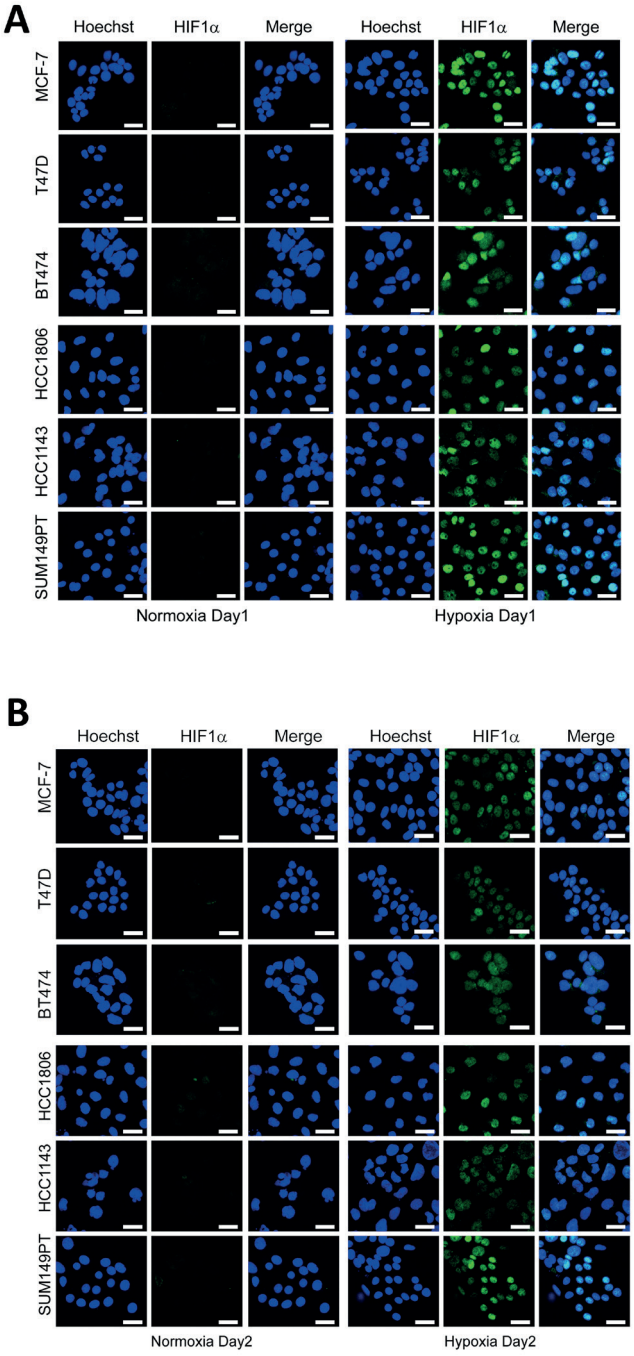

Figure S1. HIF1 accumulation in response to hypoxia in a series of luminal and basal A cell lines. (A, B) HIF1α expression and localization analyzed by confocal immunofluorescence microscopy in three luminal (MCF7, T47D and BT474) and three basal A cell lines (HCC1143, HCC1806 and SUM149PT) incubated under normoxia (21% O_2) or hypoxia (1% O_2) for 1 (A) or 2 days (B). Blue, Hoechst; Green HIF1α Ab.

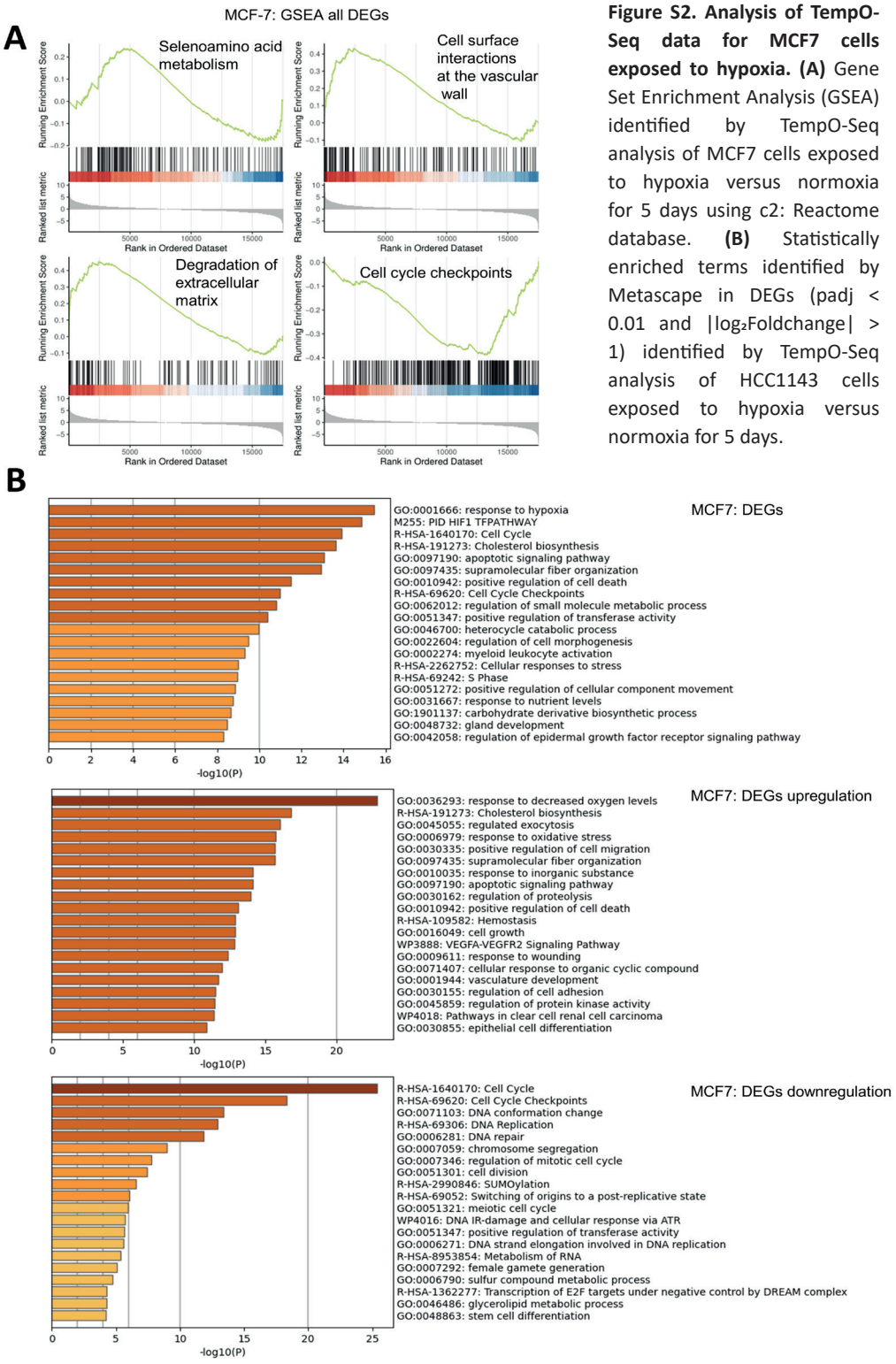

Figure S2. Analysis of TempO-Seq data for MCF7 cells exposed to hypoxia. (A) Gene Set Enrichment Analysis (GSEA) identified by TempO-Seq analysis of MCF7 cells exposed to hypoxia versus normoxia for 5 days using c2: Reactome database. **(B)** Statistically enriched terms identified by Metascape in DEGs (padj < 0.01 and $|\log_2 \text{Foldchange}| > 1$) identified by TempO-Seq analysis of HCC1143 cells exposed to hypoxia versus normoxia for 5 days.

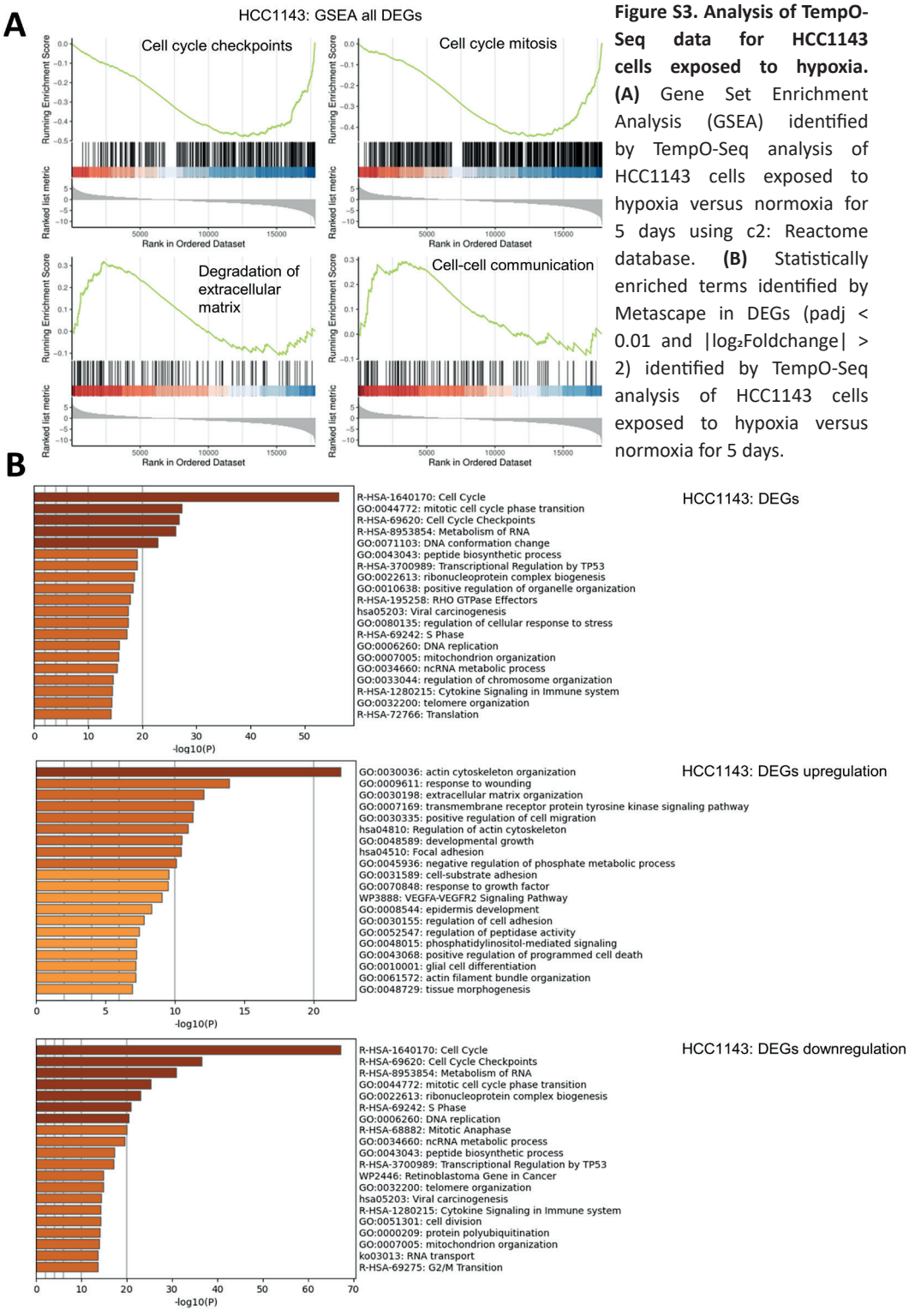

Figure S3. Analysis of TempO-Seq data for HCC1143 cells exposed to hypoxia. **(A)** Gene Set Enrichment Analysis (GSEA) identified by TempO-Seq analysis of HCC1143 cells exposed to hypoxia versus normoxia for 5 days using c2: Reactome database. **(B)** Statistically enriched terms identified by Metascape in DEGs (padj < 0.01 and $|\log_2 \text{Foldchange}| > 2$) identified by TempO-Seq analysis of HCC1143 cells exposed to hypoxia versus normoxia for 5 days.

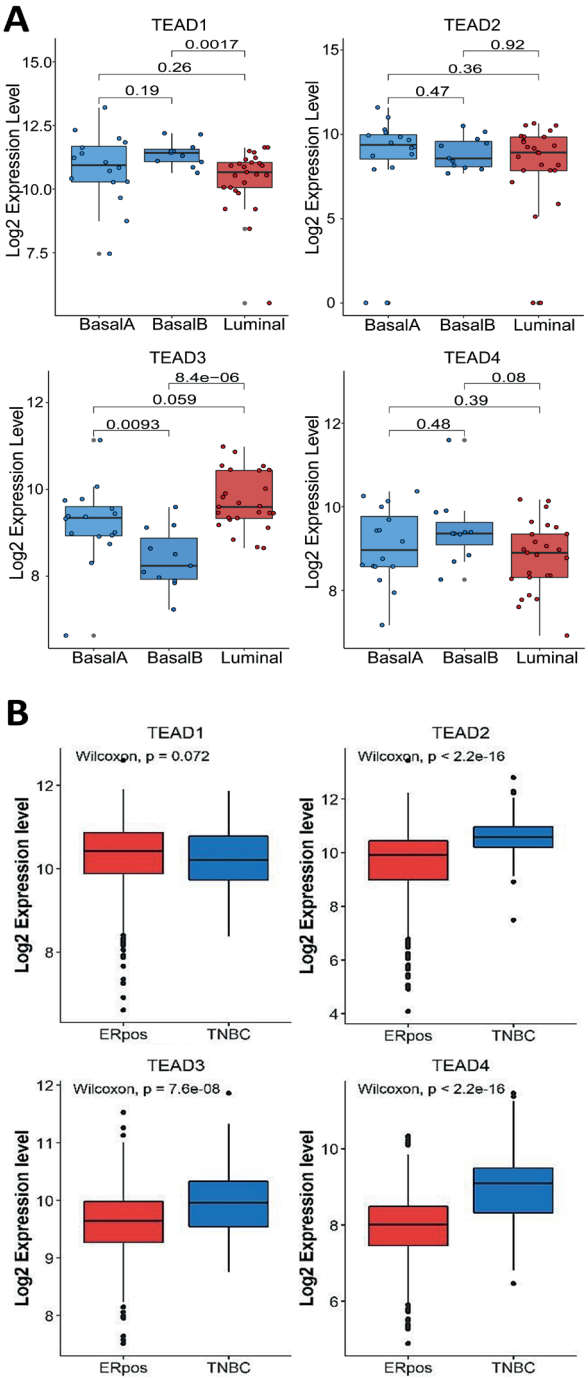

Figure S4. Expression of TEAD1-4 in breast cancer cell lines and tumors. (A) RNA expression level of TEAD1-4 from RNA-Seq data for 52 human breast cancer cell lines classified as luminal-, basal A-, or basal B-like subtype. p-value calculated using One-way ANOVA. **(B)** RNA expression levels of TEAD1-4 in ER positive and TNBC clinical samples. p-values calculated using Wilcoxon signed-rank test.

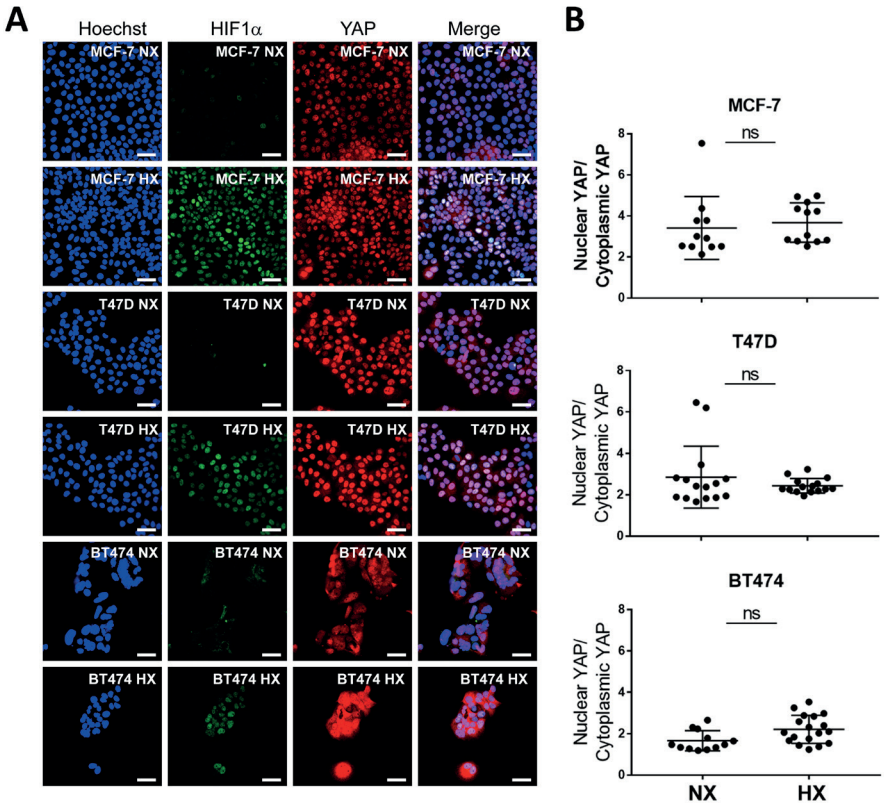

Figure S5. Localization of YAP and HIF1α in luminal cells under normoxia and hypoxia. (A) Localization of HIF1α and YAP determined by confocal immune fluorescence microscopy in MCF7, T47D and BT474 luminal breast cancer cell lines cultured under normoxia (NX) or hypoxia (HX) for 5 days. Blue, Hoechst; Green HIF1α Ab; Red, YAP Ab. **(B)** Nuclear/cytoplasmic distribution of YAP in the indicated luminal cells cultured under normoxia or hypoxia, calculated form images in A. Y-axis indicates percentage of the total intensity in the nuclei area versus percentage of the total intensity in the cytoplasm area. One representative experiment of at least three biological replicates is shown.

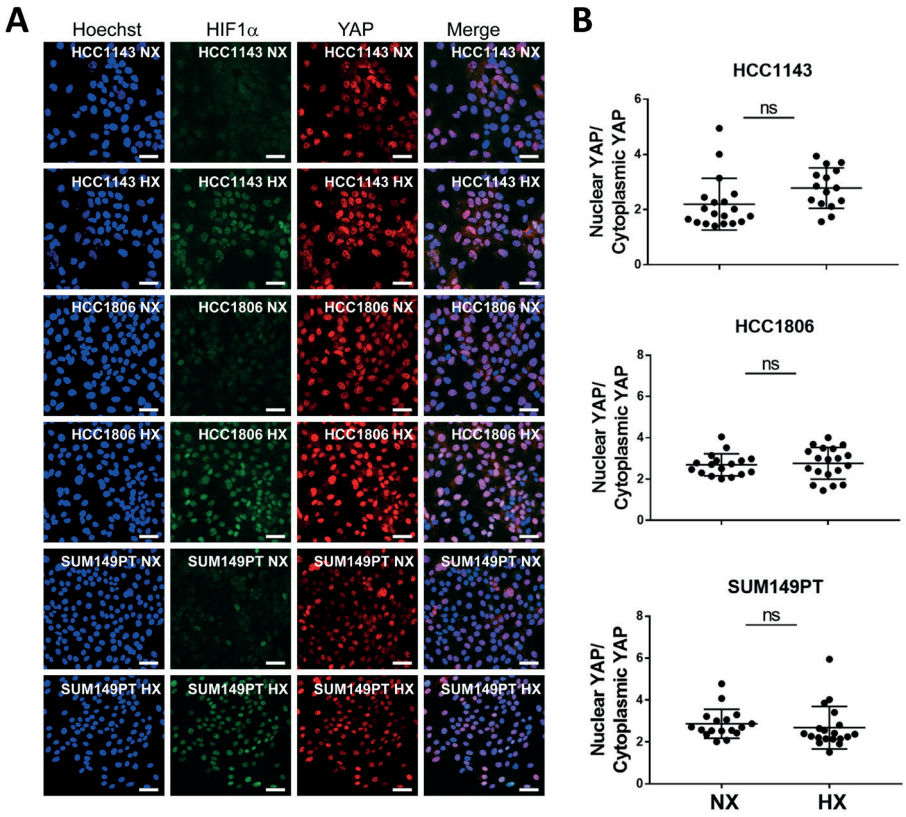

Figure S6. Localization of YAP and HIF1α in basal A cells under normoxia and hypoxia. (A) Localization of HIF1α and YAP determined by confocal immune fluorescence microscopy in HCC1143, HCC1806 and SUM149PT basal A cell lines cultured under normoxia (NX) or hypoxia (HX) for 5 days. Blue, Hoechst; Green HIF1α Ab; Red, YAP Ab. **(B)** Quantification of nuclear/cytoplasmic distribution of YAP in the indicated basal A cells cultured under normoxia or hypoxia, calculated form images in (A). Y-axis indicates percentage of the total intensity in the nuclei area versus percentage of the total intensity in the cytoplasm area. One representative experiment of at least three biological replicates is shown.